Petroleum Science 23 (2026) 1066–1088

Contents lists available at ScienceDirect

Petroleum Science

journal homepage: www.keaipublishing.com/en/journals/petroleum-science

Review Paper

Thermal maturity assessment of organic matter in the Precambrian–Lower Paleozoic high-over matured marine shale reservoirs: A review

Si-Yi Liu [a], Ping Gao [a,*], Xian-Ming Xiao [a,b], Qin Zhou [c], Yan-Ming Zhao [a], Wei Liu [a]

[a] School of Energy Resources, China University of Geosciences (Beijing), Beijing, 100083, China
[b] Frontiers Science Center for Deep-time Digital Earth, China University of Geosciences (Beijing), Beijing, 100083, China
[c] State Key Laboratory of Deep Earth Processes and Resources, Guangzhou Institute of Geochemistry, Chinese Academy of Sciences, Guangzhou, 510640, Guangdong, China

ARTICLE INFO

Article history:
Received 10 September 2024
Received in revised form
20 March 2025
Accepted 15 September 2025
Available online 19 September 2025

Edited by Xi Zhang and Jie Hao

Keywords:
Optical reflectance
Solid bitumen
Vitrinite-like maceral
Zooclasts
Raman spectroscopy

ABSTRACT

Thermal maturity is one of key parameters for source rock evaluation, which affects not only the effectiveness of hydrocarbon generation and the properties of hydrocarbon but also the formation, evolution and extinction of organic matter-hosted pores in shale reservoirs. Thus, accurate assessment of thermal maturity is of great significance to the evaluation of conventional source rocks and gas-bearing properties of unconventional shale reservoirs. However, thermal maturity assessment of the Precambrian–Lower Paleozoic marine shale deposits has been challenging for several decades. On one hand, the widely used gold standard-vitrinite reflectance (VR_o) cannot be used for maturity assessment due to the absence of vitrinite in the pre-Devonian strata. On the other hand, traditional organic geochemistry approaches (e.g., T_{max}, biomarkers) cannot be used for maturity assessment of marine shale deposits at the high-over matured stages. In this review, four groups of macerals, including solid bitumen, vitrinite-like maceral, zooclasts and liptinite, can be identified in the Precambrian–Lower Paleozoic sediments, and optical characteristics and origins of these macerals have been summarized. Furthermore, various proxies of thermal maturity assessment are systematically investigated, providing potential solutions for accurate assessment of thermal maturity of the Precambrian–Lower Paleozoic high-over matured marine shale reservoirs. However, accurate identification of different macerals (e.g., solid bitumen, vitrinite-like maceral, graptolite) is still challenged, and moreover, the use of optical reflectance of these macerals is hindered due to optical anisotropies and various conversion relationships that converted their reflectance to equivalent vitrinite reflectance ($EqVR_o$). In addition, Raman spectrometry is a rapid and non-destructive approach to evaluate thermal maturity of organic matter, and several Raman parameters, including FWHM-G, RBS and I_D/I_G ratio, can be used as the reliable maturity indicators, which overcome the influence of optical anisotropy on the optical indicators. Nevertheless, the application of Raman spectroscopy has been limited due to the lack of uniform test standards (e.g., experimental conditions) and peak fitting methods. In a word, every maturity proxy has its suitable range of application and limitations, so a variety of maturity indicators are essential to comprehensively evaluate thermal maturity of organic matter.

1. Introduction

With the urgent necessity of energy transition, unconventional shale gas is becoming the major target of hydrocarbon exploration (Liu et al., 2024; Luo et al., 2020; Montgomery et al., 2005; Rahmani et al., 2022; Zou et al., 2018). Numerous studies have investigated the structural characteristics, lithological composition, diagenesis, and pore characterization of gas shale reservoirs, as well as the occurrence states of shale gas, promoting the better

* Corresponding author.
E-mail address: gaoping1212@cugb.edu.cn (P. Gao).
Peer review under the responsibility of China University of Petroleum (Beijing).

https://doi.org/10.1016/j.petsci.2025.09.028

understanding of fine-grained sedimentary rocks (Bernard and Horsfield, 2014; Cao et al., 2019, 2020; Hackley et al., 2021; Loucks et al., 2009, 2012; Liu et al., 2022; Meng et al., 2024; Xing et al., 2023; Zhao et al., 2022). Thermal maturity can indicate the degree of thermal degradation of organic matter (OM), which also can be served as one of key indicators for evaluating the oil/gas-bearing qualities of shale reservoirs (Hunt, 1996; Jarvie et al., 2007; Mastalerz et al., 2018). When thermal maturity reaches the over-mature stage, OM-hosted pores would continue to be diminished and even disappeared at higher maturity levels, and high risks would be faced in shale gas exploration and development (Xiao et al., 2015). On the one hand, the origin, properties, quality, and quantity of hydrocarbons generated from sedimentary OM would be varied at different maturity stages (Mastalerz et al., 2018; Sanei, 2020). Since the maturity parameters (e.g., VR_o) generally display positive relationships with gas content of shale reservoirs (Hackley and Cardott, 2016; Hao et al., 2013; Mastalerz et al., 2013), thermal maturity is one of major factors influencing gas content of organic-rich shale reservoirs thus influencing the determination of favorable areas for shale gas exploration (Mastalerz et al., 2018). On the other hand, organic pores are regarded as major storage spaces for methane gas of marine shale reservoirs, so the formation, evolution, and disappearance of organic pores are unavoidably controlled by the maturity levels (Hao et al., 2013; Karg and Sauerer, 2022; Loucks et al., 2012; Borjigin et al., 2021; Xu et al., 2022; Yang et al., 2021). Therefore, accurate assessment of thermal maturity of sedimentary OM is critical for understanding the distribution of effective source rocks and high-quality shale reservoirs as well as thermal evolution and hydrocarbon potential of studied basins.

Vitrinite reflectance (VR_o) is the only one widely recognized and comparable indicator of thermal maturity (Hackley et al., 2015; Hunt, 1996). Nonetheless, the maturity level of the Precambrian to Lower Paleozoic shale deposits cannot be accurately assessed due to the lack of higher plants and associated vitrinite fragments in the pre-Devonian strata (Bertrand, 1990; Goodarzi, 1984; Goodarzi and Norford, 1985; Luo et al., 2020; Petersen et al., 2013). Besides the VR_o, some alternative indicators, e.g., Rock-Eval T_{max}, maturity-related biomarkers, fluorescence, conodont color alteration index (CAI), thermal alteration index (TAI), illite crystallinity index, etc., can also be used for thermal maturity assessment (e.g., Bertrand, 1990, 1993; Buchardt and Lewan, 1990; Hartkopf-Fröder et al., 2015; Jaboyedoff et al., 2001; Kübler and Jaboyedoff, 2000; Liu et al., 2024; Mukherjee et al., 2019; Petersen et al., 2013; Varol and Demirel, 2020). However, the Precambrian–Lower Paleozoic shale deposits usually have experienced greater burial depths and longer thermal histories and reached the high to over mature stages, thus traditional organic geochemical approaches are invalid for thermal maturity assessment (Yang and Horsfield, 2020). The CAI and TAI values have been frequently used as semi-quantitative indicators for thermal maturity assessment, thus optical reflectance has been still regarded as the mostly used and practical approach (e.g., Bertrand, 1990, 1993; Buchardt and Lewan, 1990; Petersen et al., 2013). The illite crystallinity index has been generally used as a proxy for distinguishing diagenetic stages of very low-grade metamorphism in low-temperature regionally metamorphosed areas (Jaboyedoff et al., 2001; Kübler and Jaboyedoff, 2000; Liu et al., 2024; Mukherjee et al., 2019; Varol and Demirel, 2020). However, illite crystallinity merely provides a rough range, which can be influenced by the type of clay minerals, thus leading to the relatively large errors (Kübler and Jaboyedoff, 2000). In addition, basin modelling can also be used as a complementary calibration method to reduce methodological and analytical uncertainties (Wang et al., 2023), but the uncertainties of some key geological parameters such as stratigraphic sedimentary burial history, rock thermal physical properties, and paleo-heat flow can also lead to significant deviations of output results (Wang et al., 2023). Moreover, with the increasing maturity, chemical composition and structures of the OM would progressively tend to be convergent, and different macerals could be hardly distinguished by using optical microscopy, hindering the further investigation of the origins and aromatization processes of these macerals (Luo et al., 2023).

Optical maturity indicators, e.g., solid bitumen reflectance (SBR_o), vitrinite-like maceral reflectance ($VLMR_o$), and graptolite reflectance (GR_o), have been widely used for thermal maturity assessment of the pre-Devonian shale succession, which can be converted to equivalent vitrinite reflectance ($EqVR_o$) (Goodarzi and Norford, 1985; Jacob, 1989; Luo et al., 2021; Schmidt et al., 2019; Wu et al., 2023). Solid bitumen (SB) is the most prevalent secondary maceral in the Precambrian–Lower Paleozoic marine shale, and SBR_o has been widely used for assessing thermal maturity of sediments (e.g., Bertrand, 1990; Jacob, 1989; Landis and Castaño, 1995; Schmidt et al., 2019; Schoenherr et al., 2007). However, the results of the same sample measured by different authors can be widely varied, which have been usually accounted for the following two aspects. First, SB can be easily misidentified with other macerals when it occurs as small particles (Hackley and Cardott, 2016; Mastalerz et al., 2018; Petersen et al., 2013; Wang et al., 2019; Wei et al., 2014, 2016). Second, optical anisotropy and heterogeneity of SB can be observed at higher maturity levels (Bernard et al., 2012a, 2012b; Landis and Castaño, 1995; Loucks et al., 2009; Wang et al., 2019; Xiao et al., 2000), and particularly, abundant nano-scale pores can be developed within SB (Bernard et al., 2012a, 2012b; Cardott et al., 2015; Curtis et al., 2012; Liu et al., 2022; Mastalerz et al., 2013, 2018; Wang et al., 2019). Vitrinite-like maceral (VLM), so-called as marine vitrinite, is a primary maceral with optical properties similar to vitrinite (Buchardt and Lewan, 1990), which is commonly found in the Precambrian–Paleozoic marine shales (Buchardt and Lewan, 1990; Luo et al., 2021; Sanei et al., 2014). Graptolite is a type of zooclasts in the Lower Paleozoic marine shale, and GR_o can be used as an effective maturity indicator due to the distinctive optical characteristics and specific biological origins of the graptolite (Goodarzi, 1984; Goodarzi and Norford, 1985, 1989; Goodarzi et al., 1985; Gentzis et al., 1996; Bertrand et al., 2003; Petersen et al., 2013; Lavoie et al., 2016; Luo et al., 2016, 2017, 2018, 2020). Nonetheless, optical reflectance indicators have several limitations in both measurement and data processing. For example, the accurate identification of organic zooclasts mainly depended on the researcher's experience and expertise and appropriate conversion equations between optical reflectance and VR_o values is crucial to maturity evaluation. Therefore, the use of these indicators may lead to inaccurate assessment of thermal maturity in the Precambrian–Lower Paleozoic shale deposits (e.g., Hackley et al., 2018; Mastalerz et al., 2018; Misch et al., 2019).

Raman spectroscopy of carbonaceous materials can yield representative spectral peaks (e.g., first-order vibrational peaks: D-band and G-band) indicating the information of chemical structures (Hao et al., 2019), which has been widely used to assess the maximum temperature associated with contact and/or regional metamorphism (Rantitsch et al., 2004; Endo et al., 2012; Mathew et al., 2013; Buseck and Beyssac, 2014; Henry et al., 2019a, 2019b), and maturity levels of the OM due to the advantages of convenient, fast, and high-precision measurements (Beyssac et al., 2002; Kelemen and Fang, 2001; Liu et al., 2013; Wilkins et al., 2014). However, the unified standards, such as sample preparation, testing conditions and deconvolution, are still lacking, which have directly impacted on the widespread use of

Raman spectroscopy in assessing organic matter maturity (Henry et al., 2019a).

Currently, primary approaches evaluating thermal maturity of the Precambrian–Lower Paleozoic high-over mature marine shale deposits include optical reflectance (e.g., SBR_o, $VLMR_o$, and GR_o) and the Raman spectral parameters. In order to acquire more complete and reliable maturity results, the advantages and shortcomings of various maturity approaches should be comprehensively evaluated. Therefore, the objectives of this review are to (1) characterize the different macerals in Precambrian–Lower Paleozoic shale, mainly including solid bitumen, vitrinite-like maceral, zooclasts, and liptinites; (2) investigate the principles, application, as well as advantages and limitations of various optical reflectance parameters and Raman spectroscopy parameters; (3) conduct a comparison study of various maturity approaches, providing most reasonable ideas for accurate assessment of thermal maturity in the high-over marine shale deposits.

2. Classification and characterization of macerals in the Precambrian–Lower Paleozoic shales

Macerals in sedimentary rocks are the fundamental materials for hydrocarbon generation, which could influence the hydrocarbon potential and quality of source rocks (Hackley and Cardott, 2016; Luo et al., 2020). Meanwhile, OM occurrences and types are directly related to total porosity, pore structure evolution, and gas-bearing property of shale reservoirs, playing a crucial role in appraising the potentials of conventional and unconventional hydrocarbon resources (Hackley and Sanfilipo, 2016; Liu et al., 2022; Loucks et al., 2012; Borjigin et al., 2021; Xiao et al., 2015). However, OM compositions of the Precambrian–Lower Paleozoic sediments are principally contributed from lower organic organisms, including planktonic algae, zooplankton, and bacteria (Teichmüller, 1986; Luo et al., 2023; Xiao et al., 2000; Zhong and Qin, 1995). These organisms have experienced a long history of burial and thermal evolution and reached the overmature stage, displaying similar optical and morphological features and thus resulting in difficult identification of various macerals (Zhong and Qin, 1995). Numerous authors have proposed the definition of different macerals in organic-rich shale deposits at different ages, but there still have some differences in nomenclature of various macerals, thus hindering practical application of organic petrology (Hackley and Cardott, 2016; Luo et al., 2021, 2023; Zhong and Qin, 1995). Most recently, Luo et al. (2023) systematically studied both naturally and artificially maturated samples of the Precambrian–Lower Paleozoic sections from all over the world. Based on the optical properties (e.g., reflectance and fluorescence) and structural features (e.g., morphology and texture) of various macerals, as well as the source, genesis, sedimentary transformations, and thermal degradation processes of the OM, they established a classification and naming scheme of various macerals, i.e., solid bitumen, vitrinite-like maceral, zooclasts, liptinites and inertinites (Luo et al., 2023). In this study, we primarily refer to the classification and nomenclature scheme proposed by Zhong and Qin (1995) and Luo et al. (2023), and characterize various macerals identified from the Precambrian–Lower Paleozoic shale deposits in many sedimentary basins (Table 1).

2.1. Solid bitumen

Solid bitumen (SB) has been described by a multitude of terms, including bitumen, solid hydrocarbon, migrabitumen, reservoir bitumen, pyrobitumen, etc. (Gentzis and Goodarzi, 1990; Hackley and Cardott, 2016; Hunt, 1996; Hwang et al., 1998; Jacob, 1989; Khorasani and Michelsen, 1993; Mastalerz et al., 1995; Suárez-Ruiz et al., 2012; Tissot and Welte, 1984; Wilson, 2000). Organic geochemists define bitumen as the OM component soluble in organic solvents, which is contrast to kerogen insoluble in organic solvents (Hackley and Cardott, 2016; Hackley et al., 2021; Hwang et al., 1998; Mastalerz et al., 2018). Organic petrologists describe bitumen as secondary component formed from thermal degradation of kerogen or crude oils, and the bitumen filling in pores, voids and cracks of rocks can be easily identified using optical observations (Hunt, 1996; Li et al., 2024; Waliczek et al., 2019). In this study, the latter has been described as SB.

As a secondary maceral, SB can be formed via a verity of geological alteration processes, including thermal cracking of oils, devolatilization, and biodegradation, but there have some differences in occurrence forms and optical properties (Li et al., 2024; Liu et al., 2023). Abraham (1918) divided SB into six types based on physical features, but the genesis of SB was not considered. Subsequently, the influence of thermal maturity was introduced to the classification of SB (Jacob, 1989; Landis and Castaño, 1995), and the boundary between SB and pyrobitumen at solid bitumen reflectance (SBR_o) = 0.7%. However, since liquid hydrocarbons and their secondary products would continue to be cracked to pyrobitumen at high maturity stages, such a classification scheme should be updated (Jacob, 1989). Thus, the boundary between SB and pyrobitumen should be defined at the SBR_o = 1.5%, which can be shifted to 1.3% for sulfur-rich kerogen due to the secondary gas generation (Mastalerz et al., 2018). Zhong and Qin (1995) defined bitumen directly as secondary maceral based on its genesis. Curiale (1986) genetically classified SB as pre-oil SB and post-oil SB based on biomarkers and other geochemical analyses. Pre-oil SB is immature products of source rocks, which displays very viscous characteristics and has been migrated minimal distances to fractures. Post-oil SB is the product of the alteration of a once-liquid oil, which is generated and migrated from matured source rocks. Misch et al. (2019) categorized SB into in-situ SB and migrated SB based on secondary migration. Since the definition of migration distance was ambiguous, Sanei (2020) further proposed a new schematic model for generation and timing of multiple phases of SB throughout the continuum of OM maturation in source and tight reservoir based on genesis and thermal maturity, i.e., diagenetic SB (or degraded bituminite), initial-oil SB, primary-oil SB, late-oil SB (solid-wax) and pyrobitumen. Luo et al. (2023) divided SB in the Precambrian–Lower Paleozoic sedimentary rocks into three categories, including thucholite, in-source SB and reservoir SB. Thucholite consists of radioactive mineral particles and bitumen, which generally displays sub-rounded to rounded and irregular shapes, with a diameter of about tens of micrometers (Fig. 1(a) and (b)). SB around the radioactive particles generally displays the decreasing optical reflectance from inside to rim (Crick, 1992; Crick et al., 1988; Luo et al., 2014, 2023). In-source SB occurs in source rock without long distance migration, while reservoir SB is commonly found in reservoirs such as carbonate rocks and sandstones after secondary migration (Luo et al., 2023). In summary, the classification of SB is mainly based on the following aspects: one is different properties of SB during thermal evolution; another is occurrence states based on whether SB has been migrated or not (Liu et al., 2023). However, SB in the high-over mature shale reservoirs is mostly formed via complex chemical alterations of some original macerals under the conditions of high temperature and pressure, which may have not migrated over long distances (Fig. 1(c)–(f)).

SB often belongs to the prevalent OM component of in the Precambrian–Lower Paleozoic high-overmature shale (e.g., Hackley and Cardott, 2016; Mastalerz et al., 2018; Rippen et al., 2013). Unlike primary macerals, SB generally occupies the voids or pore spaces of shale reservoirs thus displaying amorphous

Table 1
Classification of various macerals in the Precambrian–Lower Paleozoic shales (modified from Luo et al. 2023).

Maceral group	Maceral	Descriptions	Applicable age range
Solid bitumen (SB)	In-source solid bitumen	Solid-phase secondary products remaining in the source rock after the petroleum migration	Precambrian–Paleozoic
	Thucholite	Polymerized algal OM subjected to ionic radiation from radioactive minerals	/
Vitrinite-like maceral (VLM)	Vitrinite-like particle	Degraded OM formed from the humification or strong bacterial degradation that selectively degrade the active hydrogen-rich component in marine lower organisms	Precambrian–Lower Paleozoic
Zooclasts	Graptolite	Transformation products of the OM within the periderm, organic-walls and bones of marine zooplanktons	Silurian–Ordovician
	Chitinozoan		Ordovician–Devonian
	Radiolarian		/
Liptinite	Lamalginite	OM formed from degradation products of algal products and bacterial biomass	/
	Bituminite		
	Matrix-bituminite		

shapes, e.g., polygonal, clumps, bands, stripes, and irregular shapes (Fig. 1(c)–(f)). Thus, it's hard to accurately identify SB according to its morphology and occurrence forms (Mastalerz et al., 2018). Optical properties, including texture and reflectance, represent a robust method for the identification of SB particles (e.g., Goodarzi and Macqueen, 1990; Jacob, 1985; Khavari-Khorasani, 1983). Based on these properties, SB can be divided into three types: homogeneous, granular, and anisotropic (Landis and Castaño, 1995). Homogeneous SB particles have a consistent flat, smooth surface and uniform reflectance, which are ideal targets for reflectance measurement (Landis and Castaño, 1995; Mastalerz et al., 2018). Granular SB particles typically have rough surfaces, lower reflectance and display the gray-white or gray-yellow reflected light, which occur in association with homogeneous SB or widely disperse throughout the mineral matrix of the Precambrian–Lower Paleozoic high-over mature shale (Fig. 1(c)–(f)) (Mastalerz et al., 2018; Liu et al., 2023; Luo et al., 2023; Sanei, 2020). Anisotropic SB, also referring to reservoir SB or migrated SB, displays a variety of optical texture, e.g., fine-grained mosaic, coarse flow mosaic, domain and fibrous textures, which is not typical in shale reservoirs but usually occurred in carbonate rocks or sandstones (Gao et al., 2018; Goodarzi et al., 2024; Liu et al., 2023; Luo et al., 2023; Stasiuk, 1997; Zuo et al., 2022a, 2022b).

2.2. Vitrinite-like maceral

Vitrinite-like maceral (VLM) is a type of autochthonous, syndepositional, and dispersed OM, which is ubiquitous in the Precambrian–Lower Paleozoic shale deposits (Wu et al., 2023; Xiao et al., 2000). Buchardt and Lewan (1990) firstly discovered one type of OM very similar to vitrinite particles in morphology in the Cambrian-Ordovician Alum shale deposits from Northern Europe, which had been termed as "vitrinite-like maceral". Subsequently, VLM was also known as "marine vitrinite" (Zhong and Qin, 1995). VLM displaying the rounded or lenticular-elongated shapes has regarded to be primary origin, which always shows clear outlines and smooth surfaces devoid of internal textures (Fig. 2(a)–(f)). Moreover, it can be easily identified under optical microscope, which displays brown colors under transmitted light, dark gray to grayish-white colors under reflected light, and non or weak fluorescence under fluorescent reflected light (Fig. 2(c) and (d)) (Xiao et al., 2000). It exhibits the strong optical anisotropy at the overmature stage (Fig. 2(e) and (f)) (Luo et al., 2021; Wu et al., 2023).

The origins of VLM remain controversial, which have been accounted for four major opinions. (1) VLM belongs to SB, which is lack of void-filling properties and only optically similar to the vitrinite (Hackley et al., 2018; Schmidt et al., 2019). Schmidt et al. (2019) observed some overlapping data of the SBR_o and vitrinite-like maceral reflectance ($VLMR_o$) both in naturally and artificially matured samples when the maturity levels were similar. Furthermore, they noted a similar increasing trend between the $VLMR_o$ and SBR_o values during artificial maturation, implying that VLM may belong to SB. However, Luo et al. (2021) found that some VLM were encapsulated by bituminite in the Precambrian–Cambrian overmature shale deposits, and moreover, VLM and bituminite particles displayed different optical anisotropies (Fig. 2(c) and (d)), indicating that the VLM could be categorized as original maceral rather than aggregates of in-source SB. (2) VLM is a part of organic zooclasts, including graptolites and chitinozons (Goodarzi, 1984; Goodarzi and Norford, 1985; Petersen et al., 2013). Petersen et al. (2013) suggested that a part of VLM in the Alum shale may be derived from graptolite fragments, which displayed similar optical characteristics of graptolite with increasing burial depth and temperature. (3) VLM is formed via the gelification of polysaccharides of multicellular algal seaweeds, fungal hyphae, and arthropod cuticle (Buchardt and Lewan, 1990). Buchardt and Lewan (1990) suggested that the evolutionary pathway of VLM followed that of suppressed-vitrinite rather than coal-vitrinite in hydrous pyrolysis experiments, indicating that VLM may be derived from organic remains enriched in polysaccharides, such as cellulose, alginic acid, pectin, and chitin. Similarly, Xiao et al. (2000) suggested that VLM in the Cambrian-Ordovician source rocks form the Tarim Basin were mainly formed from the gelification of algal OM, because they were rich in hydrogen and exhibited a similar outline and size with multicellular algae. (4) VLM is derived from the degradation of marine lower organisms (e.g., planktonic algae) (Khan et al., 2020; Luo et al., 2014, 2021; Wang et al., 1996; Wu et al., 2023; Xiao et al., 2000; Zhong and Qin, 1995). For example, Wang et al. (1996) believed that VLM in the Lower Paleozoic high-over mature source rocks were mainly derived from the residues during thermal degradation of algae and its derivatives, and moreover, the formation and evolution of VLM can be clearly observed according to the thermal simulation of immature algal materials. Based on stable carbon isotopic compositions of various organisms and humic acids in diverse sedimentary environments, Zhong and Qin (1995) suggested that the humification of the OM could also occur in marine environments, and found that marine lower organisms could be transformed into VLM materials via marine humification under moderately oxygenated environments according to the atomic H/C and O/C ratios of marine humic acids and VLM from different basins. However, Luo et al. (2021) found the 25-norhopane, an indicator of substantial biodegradation, in the Precambrian VLM-bearing sediments, and an evolutionary pathway of "lamalginite → bituminite → VLM" during the artificial maturation of algal materials was proposed. They suggested that VLM in Precambrian shales may be formed as a result of strong bacterial degradation (e.g., sulfate-reducing bacteria and methanogens) of the lamalginite/

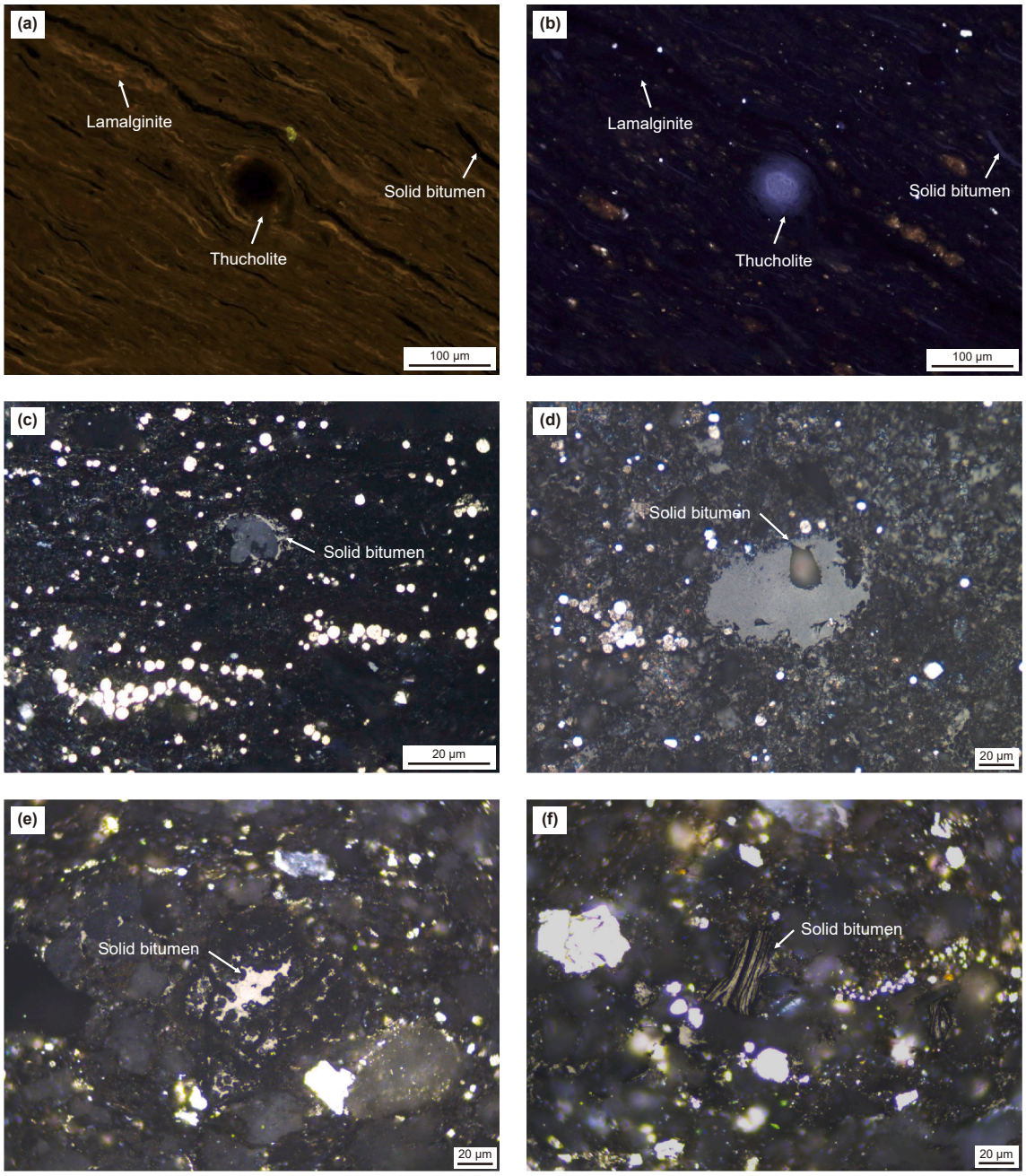

Fig. 1. Microphotographs of various types of the SB in source rocks. All microphotographs (excluding Fig. 1(a)) were captured under oil immersion reflected light. **(a–b)** The thucholite displaying halo characteristics was closely associated with the lamalginite (indicated by yellow fluorescence) and the SB along the bedding planes in the Ediacaran Salt Range Formation shale from the Indus Basin (Khan et al., 2020). **(c)** The amorphous SB displaying the weakly reflected light surrounds a granular mineral particle in the Cryogenian Dalongpo Formation black shale from the South China (Ai et al., 2021). **(d)** The granular SB has rough interior and granular mosaic texture with indistinct edges in black shale of the Ordovician-Silurian Wufeng-Longmaxi formations (WF-LMX). **(e)** The amorphous SB with fuzzy edges filled in the intergranular pores of mineral particles in the Lower Cambrian shale from the South China. **(f)** The layered SB displaying the weakly reflected light developed among clay platelets of the Lower Cambrian Qiongzhusi Formation shale from the South China.

bituminite under anoxic environments (Luo et al., 2021). The anaerobic bacterial degradation process occurs in the water column or within the sediments, which can selectively degrade the active hydrogen-rich component of the kerogen, thereby enriching the residual kerogen with higher contents of stable carbon (Khan et al., 2020; Luo et al., 2014; Machel, 2001; Sanei et al., 2014).

In summary, the origin of VLM remains unclear. Nevertheless, it is believed that VLM, as a primary maceral, is neither an aggregate of SB particles nor a part of zooclasts due to the lack of distinct biological structures, which may be originated from the humification of marine lower organisms under the moderately oxygenated conditions or selective bacterial degradation of marine organisms in anoxic environments resulting in the loss of active hydrogen-rich components, finally displaying similar optical characteristics with the vitrinite.

2.3. Zooclasts

Zooclasts refer to the optically visible carbonized residuals of various types of animals (Zhong and Qin, 1995). Three types of

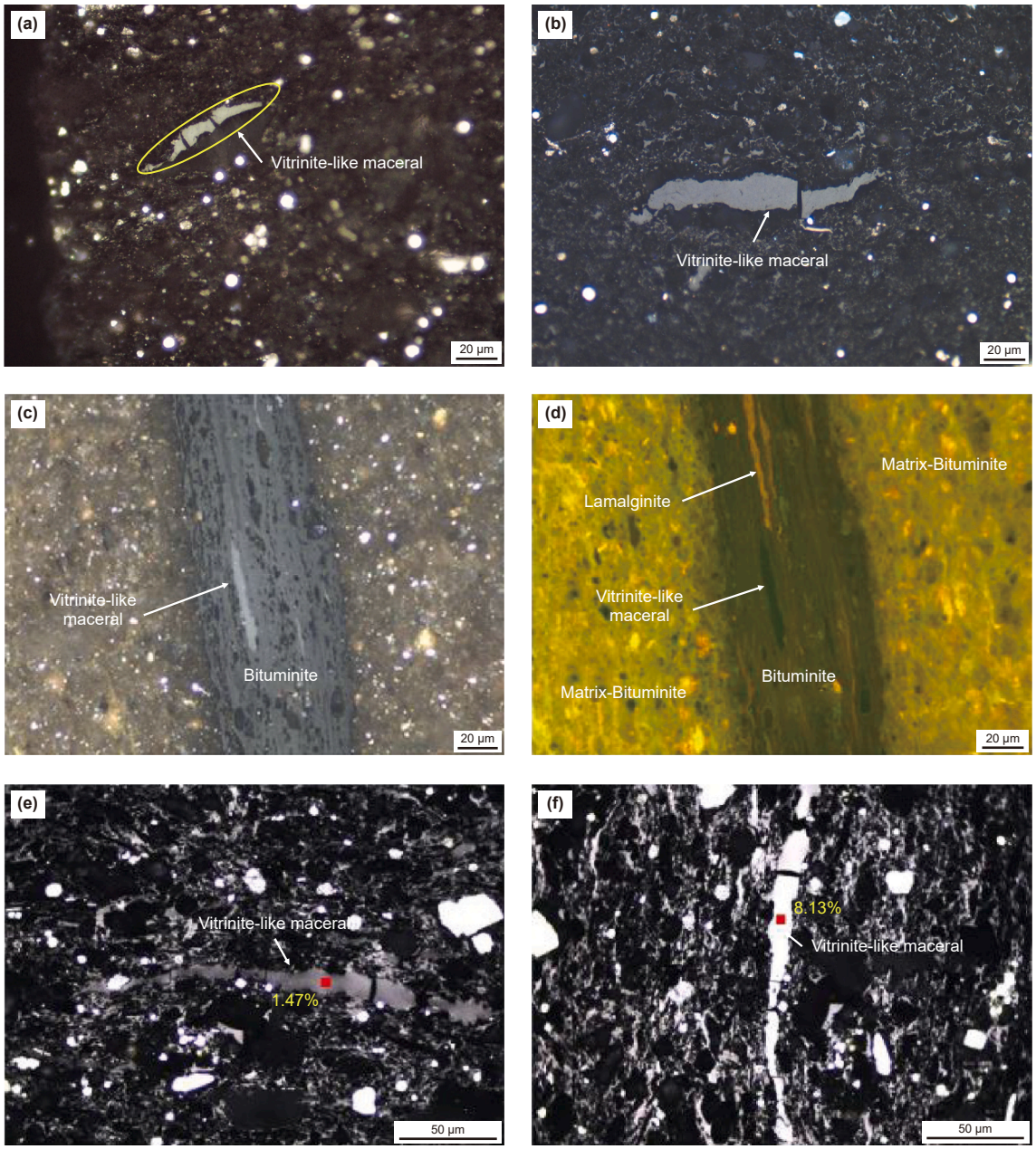

Fig. 2. Microphotographs of various types of the VLM in shales. All microphotographs (excluding Fig. 2(d)) were captured under oil immersion reflected light. **(a)** An elongated and segmented VLM particle in the Lower Cambrian shale in the South China. **(b)** A segmented VLM particle has a granular mosaic texture similar to the granular graptolite in the WF-LMX black shale in the South China. **(c–d)** Different optical and fluorescence characteristics between the VLM and other macerals (e.g., lamalginite and bituminite) of the Mesoproterozoic Xiamaling Formation lowly-matured shale deposits (Luo et al., 2021). The striped VLM with a smooth surface displays dark brown to non-fluorescing color under the fluorescent light, and gray-white color under reflected light, while the bituminite, lamalginite, and matrix-bituminite particles display yellowish-brown colors under the fluorescent light. **(e–f)** Photomicrographs of a VLM particle in the Lower Cambrian Niutitang Formation shale display strong optical anisotropy with 90° rotation of the microscopy stage under polarized light. The vitrinite-like maceral reflectance (%) is given beside the measurement site (indicated by red square) (Wu et al., 2023).

zooclasts, including graptolite periderm, chitinozoan vesicle and radiolarian, can be mainly identified in the Precambrian–Lower Paleozoic marine shale deposits (Bertrand, 1990; Goodarzi, 1984; Goodarzi and Norford, 1985; İnan et al., 2016; Lavoie et al., 2016; Luo et al., 2023; Petersen et al., 2013; Synnott et al., 2018; Wang et al., 2019). Although major sources of the buried OM in the early Paleozoic oceans have been generally regarded to be primary producers (e.g., phytoplankton; Luo et al., 2023), recent studies have found that some zooplanktons, e.g., graptolite (Fig. 3(a)–(f)), chitinozoan (Fig. 3(g) and (h)), and radiolarian (Fig. 3(i)), can have an important contribution to the buried OM in Lower Paleozoic shale deposits (Ardakani et al., 2018; Luo et al., 2016, 2020, 2023; Obermajer et al., 1996, 1999).

2.3.1. Graptolite

Graptolite is a type of marine zooplanktons, mainly living in the early Paleozoic oceans (Clarkson, 1981), which can be widely found in the Lower Paleozoic shale deposits around the world (Ardakani et al., 2018; Goodarzi, 1984; Luo et al., 2020; Reyes et al., 2018). Rhabdosome (colony) with more than one branch (stipe) is the major biological structure of graptolites, which is generally consists of fusellar tissue and cortical tissue (Luo et al., 2020). The

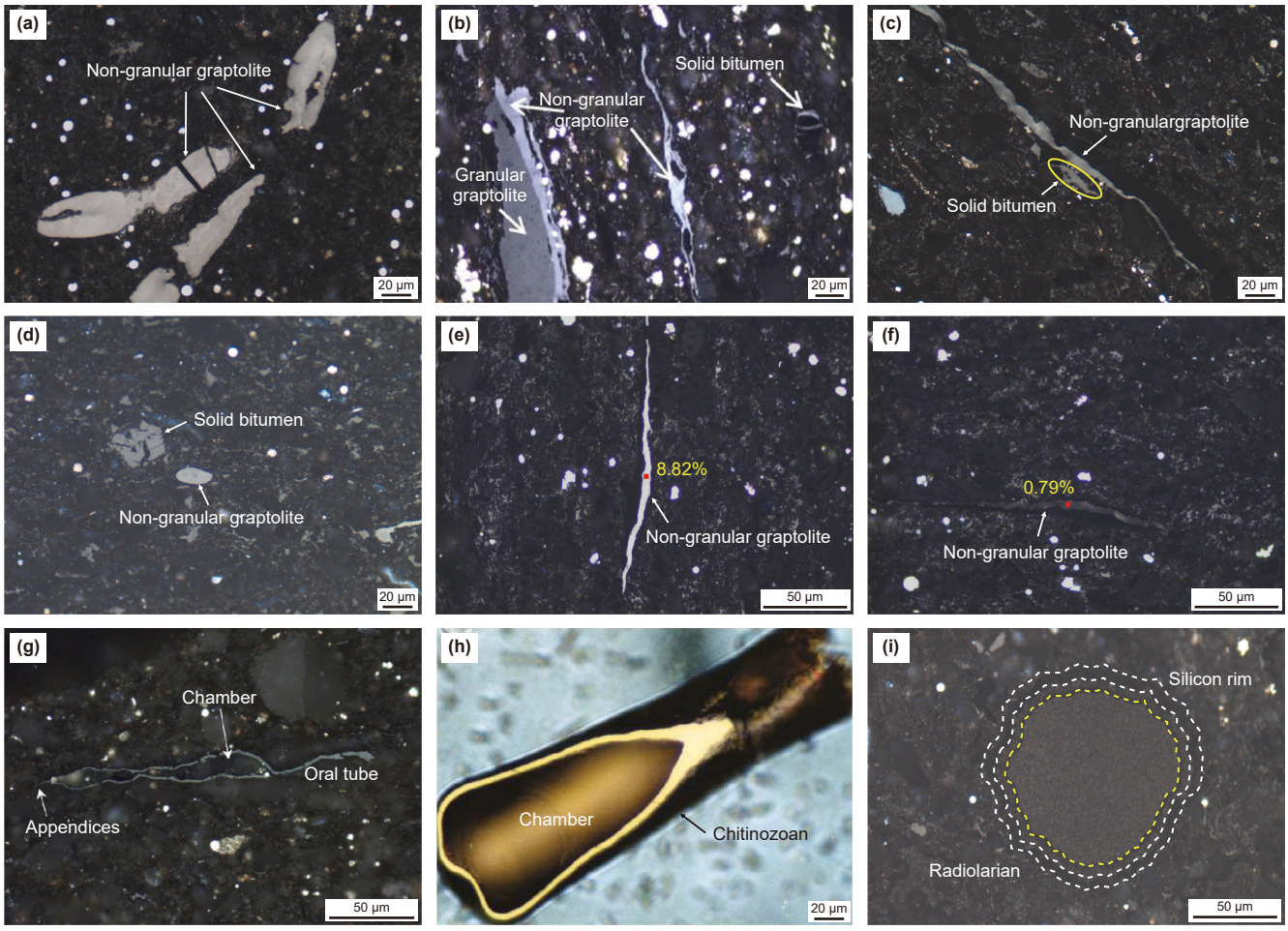

Fig. 3. Microphotographs of various types of the zooclasts in source rocks. All microphotographs were captured under oil immersion reflected light. **(a)** The elongated NGG particles have concentric layer structures and high reflectance characteristics in the WF-LMX black graptolitic shale. **(b)** The NGG and GG particles were closely associated with each other and distributed along the bedding planes of the WF-LMX shale (Luo et al., 2018). **(c)** An elongated NGG particle and associated with the SB seemed to be distributed along the bedding planes of the WF-LMX black graptolitic shale. **(d)** A blocky-shaped NGG particle in the WF-LMX shale displays the spindle-like concentric layer structure and has higher reflectance values relative to the SB. **(e–f)** High bireflectance were displayed in one same NGG particle from the WF-LMX shale in sections perpendicular to bedding when the microscope stage was rotated at 90° under polarized light. The graptolite reflectance (%) is given beside the measurement site (indicated by red square). **(g)** A chitinozoan with complete biological structures, including oral tube, chamber, and appendices from the Utica Shale (Ardakani et al., 2018). **(h)** A chitinozoan clast with the chamber in the Ekwan River Formation shale (Bertrand and Malo, 2012). **(i)** A radiolarian fragment consisting of fine-grained OM in the interior and chalcedony in the rim has been widely found in the WF-LMX shale, and the interior OM displays the characteristics of growth bands (Liu et al., 2022).

individual zooids are situated along a stipe and connected by a stolon through a common canal. The fusellar layers, thecae and common canal can be observed under optical reflected light (Fig. 3(a)) (Clarkson, 1981; Crowther, 1981; Moore, 1995).

Based on optical characteristics, the graptolite can be classified into granular graptolite (GG) and non-granular graptolite (NGG) (Fig. 3(b)). The GG generally displays fine-grained mosaic textures under reflected light and has weaker anisotropy and lower reflectance relative to the NGG (Fig. 3(b)), which has often been found in carbonate source rocks (e.g., Goodarzi and Norford, 1985). The NGG generally displays optically homogeneous textures with lath or blocky shapes (Fig. 3(c)–(f)), which is often found in mudstone source rocks (Goodarzi, 1984). The NGG may display a long stripe-like shapes in slices perpendicular to bedding planes (Fig. 3(c)). However, it sometimes shows blocky shapes in slices parallel to bedding planes, and a spindle-like concentric layer structure can also be clearly observed (Fig. 3(d)) (Link et al., 1990; Luo et al., 2017, 2020; Zheng et al., 2022). Generally, the anisotropy of NGG will increase during thermal maturation based on the positive correlation between GR_{omax} and graptolite bireflectance (Fig. 3(e) and (f)) (Luo et al., 2017), which may be related to the varying molecular structures of organisms (Goodarzi and Norford, 1985).

Regarding the origins of the GG and NGG particles, some authors hypothesized that the both were derived from different parts of rhabdosome, e.g., the common canal and the shell with fusellar layers (Goodarzi, 1984). However, Luo et al. (2018) found that the soft GG could transform into the hard and brittle NGG at the GR_o reaching 1.24% based on artificial thermal maturation of the Estonian Alum Shale, indicating that the NGG can be derived from GG under the effect of thermal stress (Luo et al., 2018). Although the graptolite contains less nanopores relative to SB, chemical composition and organic geochemical characteristics of the former show that the graptolite is mainly gas prone and has great potentials of hydrocarbon generation (Bustin et al., 1989; Cardott and Curtis, 2018; İnan et al., 2016; Liu et al., 1996; Luo et al., 2020; Wang et al., 2017).

2.3.2. Chitinozoan

Chitinozoan vesicle is derived from the hollow organic vesicles of the chitinozoans, which has morphological details like bottle or flask shapes with an oral tube, chamber, and appendice and are

common in the Ordovician–Devonian marine deposits (Fig. 3(g) and (h)) (Grahn and Paris, 2011). Chitinozoan reflectance is a powerful method of thermal maturity assessment in Lower Palaeozoic rocks (Goodarzi et al., 1985; Bertrand, 1990; Tricker et al., 1992; Petersen et al., 2013; Hackley and Cardott, 2016; Reyes et al., 2018). Due to the limited distribution of chitinozoan, however, it is difficult to obtain sufficient reflectance data, hindering the extensive use of chitinozoan reflectance. Chitinozoan vesicle displays a relatively homogeneous optical texture at low maturity stages, while it shows strong optical anisotropy and optically wavy extinction like graptolite at higher maturity stages (Fig. 3(g) and (h)) (Bertrand and Malo, 2012; Ardakani et al., 2018). Although some sporadic fractures of variable sizes remained in chitinozoans, no significant organic pores could be observed in chitinozoans at the varying maturity stages from "peak oil" to "dry gas window", implying non-porous chitinozoan walls (Ardakani et al., 2018). Meanwhile, Dutta et al. (2013) suggested that chemical compositions of chitinozoan were similar to those of Type III kerogen and gas-prone bio-macromolecules.

2.3.3. Radiolarian

Siliceous radiolarian, a lower zooplankton with siliceous skeletons, has been frequently found in the Lower Paleozoic shale deposits (De Wever et al., 2002; Liu et al., 2022; Lu et al., 2016; Tan et al., 2020). Radiolarian fragments displaying the rounded or fragmented shapes usually contain OM in the interior and chalcedony rim under optically reflected light (Fig. 3(i)) (Gao et al., 2022, 2024). The interior OM appears to display the fine-grained mosaic textures, but SEM observations have revealed that such a false appearance was resulted from the mixture of fine-grained OM (probably SB) particles and microcrystalline or nanocrystalline quartz (Gao et al., 2022, 2024; Hu et al., 2020).

2.4. Liptinite

Liptinite is generally categorized as a type of oil prone marcels (Liu et al., 2022), including lamalginite, matrix-bituminite and bituminite (Fig. 2(c) and (d)) (Hackley et al., 2018; Luo et al. 2023; Wu et al., 2023). Lamalginite is very easy to be distinguished under the reflected light, which displays yellowish to brown fluorescence with filamentous shapes and develops along the bedding planes (Fig. 2(c) and (d)) (Kus et al., 2017; Luo et al., 2023). Bituminite (so-called amorphous OM, sapropelinite or amorphinite; Hackley and Sanfilipo, 2016; Mukhopadhyay et al., 1985; Van Gijzel, 1981) is intimately intermingled within the mineral matrix, displaying amorphous or strip shapes and variable fluorescence at low-medium maturity levels (Fig. 2(c) and (d)) (Luo et al., 2023; Taylor et al., 1998; Taylor and Liu, 1989), which may be the decomposition products of marine algal bodies and planktonic debris (Goodarzi et al., 2022). Sometimes, bituminite occurs in a continuum with the organic-leaner "mineral bituminous groundmass", as known as matrix-bituminite (Fig. 2(c) and (d)) (Hackley et al., 2018; Taylor et al., 1998). It's widely accepted that the bituminite may be formed from the degradation of algal materials and bacterial biomass, which has regarded to have the greatest potentials of hydrocarbon generation (Hackley et al., 2018; Pickel et al., 2017; Taylor et al., 1998). Liptinite can be converted in-situ to SB during thermal maturation (Hackley et al., 2018), resulting in gradual disappearance of biogenic structure and fluorescence features at higher maturity stages. Therefore, liptinite is commonly observed in immature to early mature source rocks (Hackley et al., 2018), but the original outlines of biological organisms can be roughly observed sometimes (Liu et al., 2022). In a word, the occurrence of liptinite in the highly-matured shale reservoirs is still disputed.

3. Optical reflectance of different macerals

Until now, three major macerals, including SB, VLM and NGG, have been commonly selected as the ideal targets for optical reflectance measurements to evaluate thermal maturity of the Precambrian–Lower Paleozoic high-over mature shale reservoirs (e.g. Buchardt and Lewan, 1990; Jacob, 1989; Landis and Castaño, 1995; Petersen et al., 2013; Riediger, 1993; Schoenherr et al., 2007; Xiao et al., 2000; Zhong and Qin, 1995). Although other recognizable macerals (e.g., chitinozoan) can also be used as potential targets for maturity evaluation (Bertrand, 1990), they will not be discussed in this review due to the relatively low research levels, as well as less distribution in shale deposits. Therefore, three major optical reflectance indicators, as well as the advantages and disadvantages of these indicators, will be discussed.

3.1. Solid bitumen reflectance

It's widely accepted that SB is the dominant maceral in the majority of high-over mature shale deposits (Hackley and Cardott, 2016), and solid bitumen reflectance (SBR_o) has also regarded to be a reliable maturity indicator (e.g., Cardott et al., 2015; Hackley and Cardott, 2016; Mastalerz et al., 2018; Petersen et al., 2013; Reyes et al., 2018; Wei et al., 2016).

As mentioned above, SB is mainly derived from the thermal cracking of kerogen or retained hydrocarbons in shale reservoirs under high temperatures, belonging to the secondary maceral (Curiale, 1986; Mastalerz et al., 2018), and the SBR_o values increase with increasing thermal maturity (Hackley et al., 2015; Petersen et al., 2013; Riediger, 1993; Valentine et al., 2014). However, SB and vitrinite display the different evolutionary pathways, e.g., different increase rates of optical reflectance at different maturity stages (Liu et al., 2019). Numerous studies have shown that the SBR_o values were typically lower than the corresponding VR_o values at low maturity stages (VR_o < 1.0%–1.5%) (e.g., Hackley and Lewan, 2018; Schmidt et al., 2019). Since SB is a product of oil cracking, it contains large amounts of aliphatic compounds thus theoretically resulting in low aromaticity and relatively low reflectance relative to the vitrinite (Curiale, 1986; Wei et al., 2016). With the increasing maturity, the aromaticity of SB increases (Landis and Castaño, 1995), and SB and vitrinite display a similar evolutionary pathway at the VR_o > 1.0%–1.5% (Hackley and Lewan, 2018; Liu et al., 2019; Wang et al., 2020).

The conversion of the SBR_o and VR_o values plays a critical role in maturity evaluation, which has received much attention until now (e.g., Bertrand, 1990; Jacob, 1989; Landis and Castaño, 1995; Schmidt et al., 2019; Schoenherr et al., 2007). As early as 1989, Jacob (1989) proposed an empirical equation between the SBR_o and VR_o values for the migrated SB in carbonate reservoirs, but the measured SBR_o values were less than 2.5%. Subsequently, numerous authors have proposed a variety of empirical equations between the SBR_o and $EqVR_o$ values of various lithologies (e.g., carbonates and mudstone) from global sedimentary basins (Table 2; Fig. 4(a)). For example, Landis and Castaño (1995) measured the reflectance values of the vitrinite and associated homogeneous SB particles in source rocks from several sedimentary basins around the world, and proposed an empirical equation between the SBR_o and VR_o values, with wide applicable conditions (0.5% < VR_o < 5.0%). Schoenherr et al. (2007) integrated the measured data of Jacob (1989) and Landis and Castaño (1995), and proposed an updated empirical equation between the SBR_o and VR_o values. In addition, Bertrand (1990) used the chitinozoan reflectance as an intermediate variable, and established an empirical equation between the SBR_o and $EqVR_o$ values of the

Table 2
The empirical equations for equivalent vitrinite reflectance calculation ($EqVR_o$, %) based on solid bitumen reflectance (SBR_o, %).

Empirical equations	Applicable conditions	Materials/age/area	References
$EqVR_o = 0.679SBR_o + 0.3195$	$SBR_o \leq 5.0\%$	Permian and Triassic oil shale in China	Feng and Chen (1988)
$EqVR_o = 0.618SBR_o + 0.40$	$SBR_o < 2.5\%$	Carbonate rocks from Germany and undisclosed countries	Jacob (1989)
$EqVR_o = (SBR_o + 0.03)/0.96$	Limestone	Paleozoic marine sequences in Gaspe Peninsula of Eastern Canada	Bertrand (1990)
$EqVR_o = 0.618SBR_o + 0.40$	$SBR_o < 0.52\%$	Lower Jurassic "Nordegg Member" marine rocks in Canada Sedimentary Basin	Riediger (1993)
$EqVR_o = 0.277SBR_o + 0.57$	$SBR_o \geq 0.52\%$		
$EqVR_o = (SBR_o - 0.13)/0.87$	Limestone	Ordovician to Devonian samples in the Quebec, Northwest Territories, and Yukon Territory	Bertrand (1993)
$EqVR_o = 0.668SBR_o + 0.346$	/	Carbonate rocks in China	Liu and Shi (1994)
$EqVR_o = (SBR_o + 0.41)/1.09$	$0.5\% < EqVR_o < 5.0\%$	Upper Devonian and Cretaceous samples from USA	Landis and Castaño (1995)
$EqVR_o = (SBR_o - 0.059)/0.936$	$EqVR_o > 1.5\%$	Silurian-Devonian source rocks in the Gaspé Belt basin, Canada	Bertrand and Malo (2001)
$EqVR_o = (SBR_o + 0.2443)/1.0495$	$0.5\% < EqVR_o < 5.0\%$	Data from Jacob (1989) and Landis and Castaño (1995)	Schoenherr et al. (2007)
$EqVR_o = 0.83SBR_o + 0.22$	/	Middle Devonian/lower Mississippian New Albany Shale	Wei et al. (2016)
$EqVR_o = 1.35SBR_o - 0.16$	/	Naturally-matured shale samples from China, Sweden and Estonia	Luo et al. (2018)
$EqVR_o = 0.938SBR_o + 0.3145$	$0.07\% < SBR_o < 5.40\%$	Data from Jacob (1989), Landis and Castaño (1995), Newman et al. (2013), Araujo et al. (2014), Agirrezabala et al. (2014), Mählmann and Le Bayon (2016), Wei et al. (2016) and Hackley and Lewan (2018)	Schmidt et al. (2019)
$EqVR_o = 1.125SBR_o - 0.2062$	/	Longmaxi Formation shale samples in the South China	Wang et al. (2020)

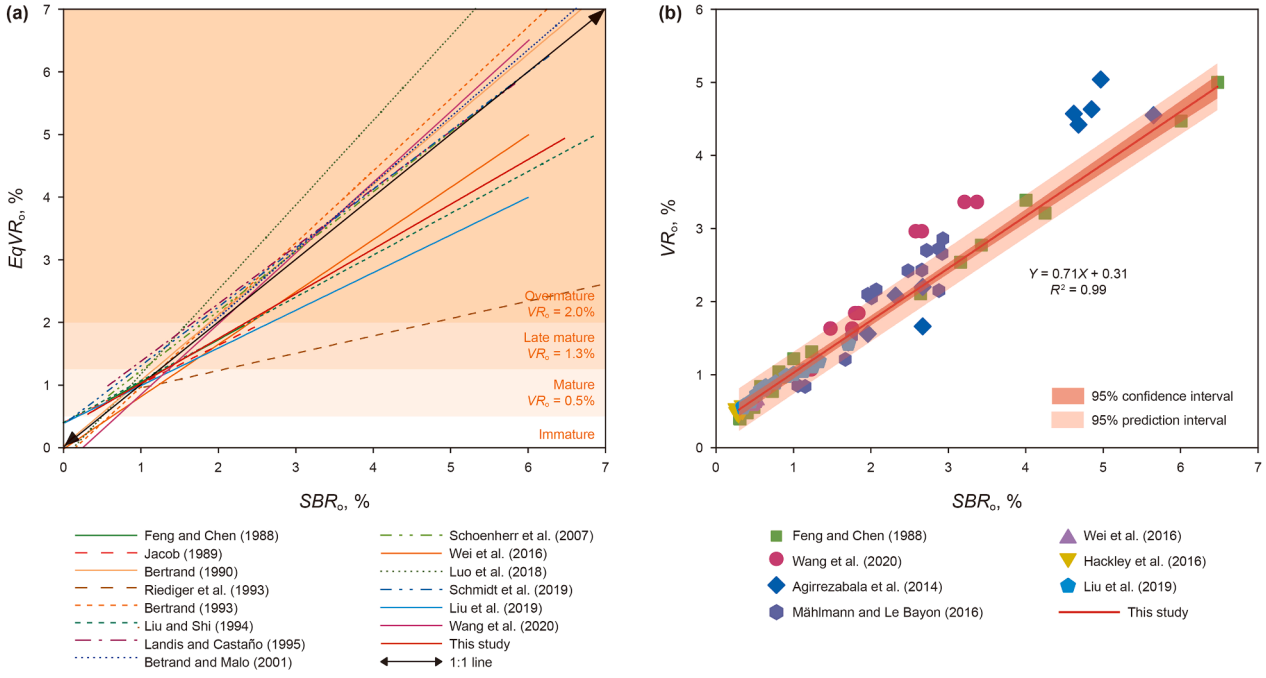

Fig. 4. The relationships between the SBR_o and VR_o or $EqVR_o$ values. **(a)** The relationships between the SBR_o and $EqVR_o$ values from previous works revealing greater differences at the overmature stage. **(b)** A cross-plot of the SBR_o versus VR_o or $EqVR_o$ values showing a new fitted empirical equation. Data are from Agirrezabala et al. (2014), Feng and Chen (1988), Hackley et al. (2016), Liu et al. (2019), Mählmann and Le Bayon (2016), Wang et al. (2020), Wei et al. (2016).

Paleozoic marine successions. Subsequently, the empirical equations between the SBR_o and $EqVR_o$ values had been updated according to different lithologies (Bertrand, 1993; Bertrand and Malo, 2001). However, practical application of these empirical equations might be challenged due to several conversions and complex origins of migrated SB. In overall, a positive linear relationship between the SBR_o and VR_o/$EqVR_o$ values seems to be displayed in majority of previous studies. However, Xiao et al. (1991) suggested that a positive linear correlation between SBR_o and VR_o/$EqVR_o$ values may only exist at the high maturity stage. Luo et al. (2021) found that the SB in the reservoir rocks have higher reflectance than that in the adjacent source rocks due to more aliphatic and aromatic hydrocarbons (Luo et al., 2021). Moreover, they have established two distinct correlation trends between SBR_o and $EqVR_o$ for the artificially matured Mesoproterozoic shale and Cambrian Alum shale samples, and such a difference may be attributed to the variations of original kerogen compositions. Additionally, an updated empirical equation between the SBR_o and $EqVR_o$ values has been established based on the large numbers of measured points from previous works (Fig. 4(b); Agirrezabala et al., 2014; Feng and Chen, 1988; Hackley and Sanfilipo, 2016; Liu et al., 2019; Mählmann and Le Bayon, 2016; Wang et al., 2020; Wei et al., 2016), which is shown in the following:

$$EqVR_o = 0.71SBR_o + 0.31 \left(n = 88;\ R^2 = 0.99\right) \quad (1)$$

Such an empirical equation can be comparable to the equation proposed by Wei et al. (2016). However, the calculated $EqVR_o$ values display large differences at the same SBR_o values, particularly at the overmature stage (Fig. 4(a)). When the SBR_o values are

given, some equations can yield lower $EqVR_o$ values (e.g., Liu and Shi., 1994; Liu et al., 2019; Riediger, 1993) whereas other equations can yield higher $EqVR_o$ values (e.g., Bertrand, 1990, 1993; Schmidt et al., 2019; Schoenherr et al., 2007). Compared with previous empirical equations, such a new equation was fitted from a variety of data sources, including naturally and artificially matured source rocks from many sedimentary basins. Meanwhile, this equation has a wide range for maturity assessment, which could essentially cover different stages of hydrocarbon generation.

3.2. Vitrinite-like maceral reflectance

VLM is an original and indigenous maceral with similar optical features to vitrinite, which is widely developed in the Precambrian–Lower Paleozoic deposits around the world (Buchardt and Lewan, 1990; Luo et al., 2021; Schmidt et al., 2015; Xiao et al., 2000; Zhong and Qin, 1995). Buchardt and Lewan (1990) firstly identified VLM in the middle Cambrian–Lower Ordovician Alum shale in southern Scandinavia. Moreover, they found that the evolutionary pathway of VLM was very similar to that of suppressed vitrinite, and VLM reflectance ($VLMR_o$) displayed a negative linear relationship with atomic H/C ratios of kerogen fractions, indicating that $VLMR_o$ may be a useful thermal maturity indicator (Buchardt and Lewan, 1990). Subsequently, some authors have conducted comprehensive investigations on the relationship between $VLMR_o$ and VR_o values (Table 3; Fig. 5(a)). For example, Cheng et al. (1995) and Wang et al. (1996) conducted artificial simulation of Lower Paleozoic lignite and kerogen samples from Ordovician Kukersite oil shale, and established a positive linear relationship between the $VLMR_o$ and VR_o values within the VR_o range of 0.73%–2.0%. Similarly, Luo et al. (2021) established a linear relationship between the $VLMR_o$ and VR_o values based on artificial maturation of the Proterozoic Xiamaling Formation shale, Cambrian Alum shale and Carboniferous coal samples. Thus, it's widely accepted that a linear relationship occurred between the $VLMR_o$ and VR_o values.

However, some studies suggested that there was a multi-stage positive linear relationship between $VLMR_o$ and VR_o values (Schmidt et al., 2015; Xiao et al., 2000). Xiao et al. (2000) had investigated the VLM in the Lower Paleozoic deposits from the Tarim Basin and found three-stage linear correlations between $VLMR_o$ and VR_o values based on artificially- and naturally-maturated samples. In contrast, Schmidt et al. (2015) suggested two-stage linear regression equations according to the naturally- and artificially-matured samples from the Ponta Grossa Formation (Middle Devonian or older).

In this study, based on large amounts of measured points from previous works (Cheng et al., 1995; Luo et al., 2021; Schmidt et al., 2015; Wang et al., 1996, 2010; Wu et al., 2023; Xiao et al., 2000), a positive linear relationship between the $VLMR_o$ and VR_o values can be clearly observed (Fig. 5(b)), and an updated empirical equation has been established in the following:

$$EqVR_o = 0.86VLMR_o + 0.37 \left(n = 103;\ R^2 = 0.93\right) \quad (2)$$

This new liner relationship is similar to Eq. (1), consistent with the empirical equation proposed by Schmidt et al. (2019), which implies that SB and VLM particle may have similar optical evolutionary paths at the high-overmature stages. Similarly, this new empirical equation covers extensive data sources, but the reliability of this equation may be reduced at the $VR_o > 3.0\%$, probably resulting from the limited quantity of previously available data (Fig. 5(b)).

3.3. Graptolite reflectance

Graptolite, a primary maceral, can be easily identified under optical microscope due to its large sizes and distinctive morphological features (Bertrand et al., 2003; Goodarzi, 1984; Goodarzi and Norford, 1985; Goodarzi et al., 1992a, 1992b, 2024; Luo et al., 2020; Petersen et al., 2013). Previous works have revealed that the physicochemical properties of graptolite are more sensitive to temperature variations, and the optical evolutionary characteristics of the graptolite are similar to those of the vitrinite (Gentzis et al., 1996; Goodarzi et al., 1992b). Since the NGG is widely developed in the Lower Paleozoic shale deposits and generally displays smooth surface and relatively homogeneous optical texture under reflected light relative to the GG (Luo et al., 2020; Petersen et al., 2013), the random reflectance of the NGG (GR_o) has been widely used as a maturity indicator of the Lower Paleozoic sedimentary rocks (Table 4) (Goodarzi and Norford, 1985; Luo et al., 2020).

Many authors have proposed a variety of empirical equations between the GR_o and $EqVR_o$ values (Fig. 6), but these equations are established by using some intermediate variables (e.g., CAI, T_{max}) (Bertrand et al., 2003; Gentzis et al., 1996; Goodarzi and Norford, 1985; İnan et al., 2016; Petersen et al., 2013; Synnott et al., 2018). For example, several authors had established the relationships between maximum reflectance of graptolite (GR_{omax}) and $EqVR_o$ values via the use of conodont alteration index (CAI), which is a semi-quantitative maturity indicator (Gentzis et al., 1996; Goodarzi and Norford, 1985). Petersen et al. (2013) proposed an

Table 3
The empirical equations for equivalent vitrinite reflectance calculation ($EqVR_o$, %) based on vitrinite-like maceral reflectance ($VLMR_o$, %).

Empirical equations	Applicable conditions	Materials/age/area	References
$EqVR_o = 0.461VLMR_o + 0.75$	$0.73\% < EqVR_o < 2.0\%$	The Cambrian and Ordovician source rocks	Cheng et al. (1995)
$EqVR_o = 0.533VLMR_o + 0.667$	$1.0\% \leq EqVR_o \leq 2.0\%$	Middle Cambrian-Ordovician carbonates and mudstones in China	Wang et al. (1996)
$EqVR_o = 1.26VLMR_o + 0.21$	$VLMR_o < 0.75\%$	Naturally and artificially matured lower Palaeozoic source rocks in the Tarim Basin	Xiao et al. (2000)
$EqVR_o = 0.28VLMR_o + 1.03$	$0.75\% \leq VLMR_o \leq 1.50\%$		
$EqVR_o = 0.81VLMR_o + 0.18$	$VLMR_o > 1.50\%$		
$EqVR_o = 0.9171VLMR_o + 0.1819$	$VLMR_o \leq 0.75\%$	Artificially-matured lower Devonian and middle Devonian samples in the Paraná Basin	Schmidt et al. (2015)
$EqVR_o = 0.8452VLMR_o + 0.3756$	$0.75\% < VLMR_o \leq 1.50\%$		
$EqVR_o = 1.07VLMR_o - 0.18$	Pre-Cambrian	Artificially-matured shale samples of the Meso-proterozoic Xiamaling Formation in China and Cambrian Alum Formation in Sweden	Luo et al. (2021)
$EqVR_o = 0.67VLMR_{omax} + 0.32$	Precambrian–Lower Paleozoic shale	Naturally- and artificially-matured shale samples from Sweden, Denmark and China	Wu et al. (2023)

Note: $VLMR_{omax}$ refers to the maximum reflectance of VLM particle.

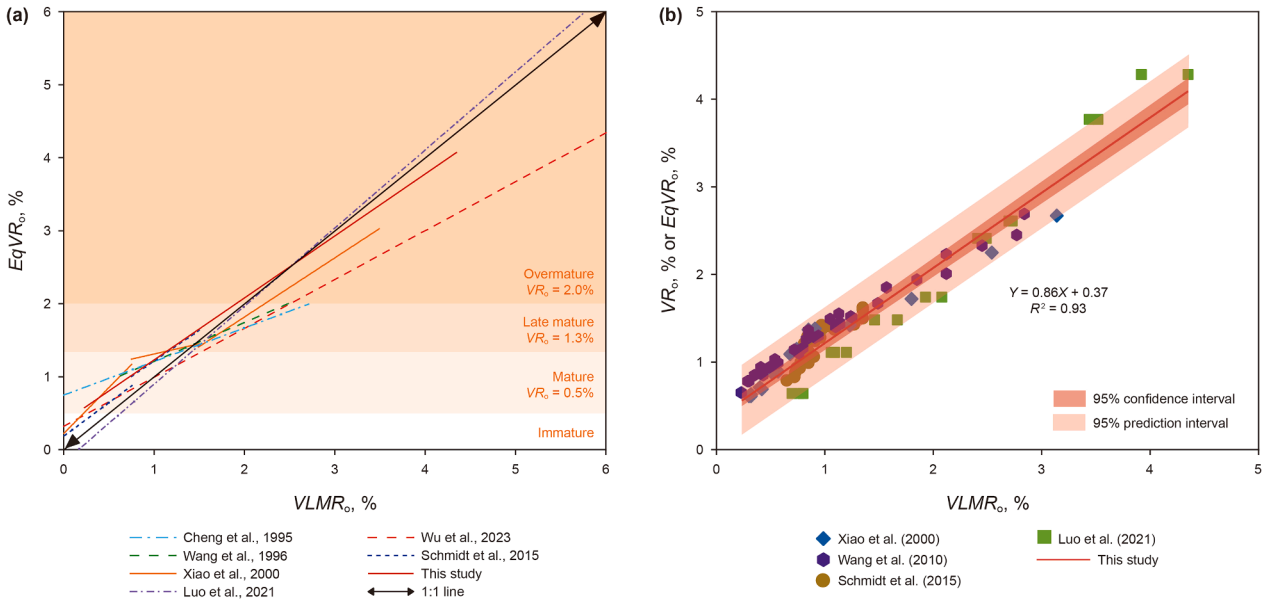

Fig. 5. The relationships between the $VLMR_o$ and VR_o or $EqVR_o$ values. **(a)** The relationships between the $VLMR_o$ and $EqVR_o$ values from previous works. **(b)** A corss-plot of the $VLMR_o$ versus VR_o or $EqVR_o$ values showing a new fitted empirical equation. Data are from Cheng et al. (1995), Luo et al. (2021), Schmidt et al. (2015), Wang et al. (1996, 2010), Wu et al. (2023), Xiao et al. (2000).

Table 4
The empirical equations for equivalent vitrinite reflectance calculation ($EqVR_o$, %) based on graptolite reflectance (GR_o, %)and chitinozoan reflectance (R_{ch}, %).

Empirical equations	Applicable conditions	Materials/age/area	References
$\lg(GR_o) = 1.1\lg(EqVR_o)-0.04$	$0.5\% < GR_o < 3.0\%$	Paleozoic marine sequences in Gaspe Peninsula of Eastern Canada	Bertrand (1990)
$GR_o = 2.113EqVR_o-0.3221$	$GR_{omax} < 5.0\%$	Lower Paleozoic sediments of the Lower Yangtze region	Zhu et al. (1998)
$EqVR_o = -0.026GR_o^2+0.524GR_o+0.5925$	GR_o	Graptolite-bearing sediments in the Tarim Basin, Ordos Basin, and Southern Jiangsu Province in China	Cao et al. (2000)
$EqVR_o = 0.5089GR_{omax}+0.4064$	$0.72\% < GR_{omax} < 4.27\%$		
$EqVR_o = 0.4168GR_{omax}-0.4655$	$5\% < GR_{omax} < 9.21\%$		
$EqVR_o = 0.9376GR_o+0.0278$	/	Silurian-Devonian source rocks in the Gaspé Belt Basin, Canada	Bertrand and Malo (2001)
$EqVR_o = 0.73GR_o+0.16$	$0.47\% < GR_o < 2.14\%$	Middle Cambrian–lower Silurian shale samples in southern and central Sweden and the Danish Island Bornholm	Petersen et al. (2013)
$EqVR_o = 1.055GR_o-0.053$	$0.65\% < GR_o < 4.03\%$	Naturally-matured shale samples from China, Sweden and Estonia	Luo et al. (2018)
$EqVR_o = 0.56GR_{omax}+0.35$	/		
$EqVR_o = 0.97GR_o-0.2$	$2.19\% < GR_o < 3.5\%$	Ordovician–Silurian naturally-matured shale samples in the South China	Wang et al. (2019)
$EqVR_o = 0.22GR_o+2.55$	$GR_o > 3.5\%$		
$EqVR_o = 0.99GR_o+0.08$	/	Graptolite-bearing sediments from the Ordovician–Silurian in China, Liteň Formation in Czech and Alum shale in Estonia and Sweden, data from Luo et al. (2018), Bertrand (1990), Bustin et al. (1989), Reyes et al. (2018)	Luo et al. (2020)
$EqVR_o = 0.75GR_o+0.64$	$GR_o \leq 3.5\%$	Ordovician–Silurian naturally-matured shale samples in the South China	Meng et al. (2022)
$EqVR_o = 0.36GR_o+2.23$	$GR_o > 3.5\%$		
$EqVR_o=(R_{ch}-0.08)/1.152$	$1\% < R_{ch} < 2\%$	Late Silurian to Devonian samples yielded chitinozoa and vitrinite collected from eight countries from three continents	Tricker et al. (1992)

Note: GR_o, GR_{omax}, GR_{omin} refer to the random reflectance, maximum reflectance, and minimum reflectance of non-granular graptolite particles, respectively. R_{ch} refer to the chitinozoan reflectance.

empirical equation between the GR_o and $EqVR_o$ values by using an intermediate variable of T_{max} values. Cao et al. (2000) used some organic geochemical indicators as the intermediate variables, and successfully established several empirical equations between GR_o/GR_{omax} and $EqVR_o$ values based on the Ordovician-Silurian shale and carbonate samples from the Tarim Basin, Ordos Basin, and South China. However, the use of intermediate variables may influence the reliability of calculated $EqVR_o$ values, particularly at the higher maturity levels, since most organic geochemical indicators will be invalid at high-over maturity stages (Bertrand et al., 2003; Gentzis et al., 1996; Goodarzi and Norford, 1985). Luo et al. (2020) presented a new correlation between GR_o and $EqVR_o$, i.e., $EqVR_o = 0.99GR_o+0.08$, based on published results as well as natural and artificial maturation of graptolite and vitrinite particles. Additionally, they suggested that chemical compositions of graptolite periderm were similar to those of vitrinite, and electron microprobe, fourier transform infrared spectroscopy (FTIR) and Raman spectrum results revealed that graptolite was prone to kerogen Type II–III (Luo et al., 2020). However, Meng et al. (2022) evaluated the maturity of the WF-LMX high-over mature shale samples in the Sichuan Basin by using the reflectance of SB and graptolite, as well as the Raman-related parameters of kerogen fractions, and found that there is not a positive linear relationship between GR_o and $EqVR_o$ values during thermal evolution (Meng et al., 2022).

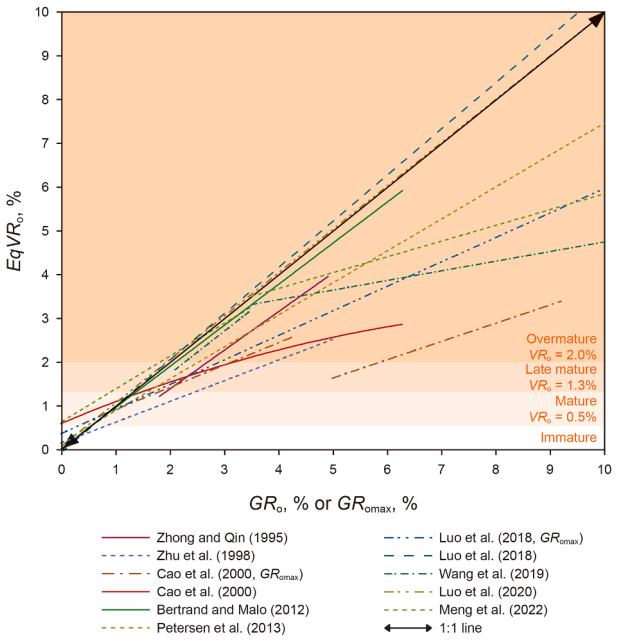

Fig. 6. The relationships between the GR_o or GR_{omax} and $EqVR_o$ values. Data are from Bertrand and Malo (2012), Cao et al. (2000), Luo et al. (2018, 2020), Meng et al. (2022), Petersen et al. (2013), Wang et al. (2019), Zhong and Qin (1995), Zhu et al. (1998).

They suggested that the graptolite displayed a similar thermal evolutionary path with the vitrinite when the GR_o values were less than 3.5%. At the $GR_o > 3.5\%$, the maturation of the vitrinite follows the graphitization trend, whereas that of the graptolite follows the original evolutionary trend (Meng et al., 2022). In a word, although there is a linear quantitative relationship between the GR_o and VR_o values, it's still doubted whether a positive linear relationship between GR_o and $EqVR_o$ values occurred.

3.4. Several challenges

Although optical reflectance parameters (e.g., SBR_o, $VLMR_o$, and GR_o) have been widely studied and used for assessing thermal maturity of the Precambrian–Lower Paleozoic highly matured source rocks, several issues still remain unsolved, hindering the application of these parameters.

(1) Accurate identification of different macerals in source rocks under optical microscope is an essential prerequisite of accurate maturity evaluation by using optical reflectance parameters, which can be only conducted by skilled and experienced researchers. SB particles dispersed in the Precambrian–Lower Paleozoic shale reservoirs generally display amorphous shapes and tiny sizes (e.g., Hackley et al., 2018; Luo et al., 2023; Wang et al., 2019), so they are hardly identified and measured, thus probably resulting in significant artificial errors. Meanwhile, the measured SB particles should be large enough, and only those particles with smooth surfaces can be used for the targets for optical reflectance measurements (Xiao et al., 1991). Compared with SB particles, VLM and graptolite particles can be easily identified due to their unique morphological features and larger sizes, thus the tasks of optical reflectance measurements may be relatively easy. However, the maturity evaluation of the Precambrian–Lower Cambrian source rocks that are devoid of VLM and graptolite particles can only be conducted by using SBR_o values.

(2) The measured reflectance values can be influenced by different pre-treatment methods of studied samples. Sanei and Ardakani (2016) found that great differences of reflectance were displayed in the shale samples polished by traditional mechanical and ion milling methods, respectively. The OM particles could be heated by ion milling processes, resulting in higher measured values of optical reflectance. In particular, SB appears to be more susceptible to thermal alteration than zooclasts (Sanei and Ardakani, 2016). Moreover, the measured GR_o values can be influenced by the orientation of the slices during sample pretreatment (Luo et al., 2020), mainly including parallel and perpendicular to bedding planes. Zhong and Qin (1995) suggested that the measurement of the GR_o values were reasonable in the slices parallel to bedding planes. Recently, Luo et al. (2020) noticed that standard deviation of the GR_o values measured from the slices perpendicular to bedding planes was smaller than those measured from the slices parallel to bedding planes, which appeared to be more accurate in case studies.

(3) The measured reflectance values can be influenced by complex properties of macerals during thermal alteration process. When the SBR_o values exceeded 1.5%–2.0%, abundant nanopores and surface imperfections can be formed in SB particles of shale reservoirs due to oil cracking and gas de-volatilization (Bernard et al., 2012a, b; Loucks et al., 2009). SEM observations have revealed that organic pores were widely developed in SB (Fig. 7(a)–(e)) as well as graptolites (Fig. 7(f)–(h)), and the occurrence of abundant nanopores and fine-grained mosaic texture would undoubtedly result in the decrease of optical reflectance. In addition, there have a false appearance on the granular mosaic texture within SB particles, which actually resulted from abundant nano-pores within SB particles, thus leading to the unreliability of measured reflectance (Fig. 7(a)–(e)). In order to avoid the effect of nanopores, Sanei et al. (2015) found that a probe size of 1.7–2.8 μm^2 was optimal for optical reflectance measurements, which can provide a reading area sufficiently small to mitigate surface imperfections and maintain an acceptable level of standard deviation. Meanwhile, optical anisotropy of VLM and NGG particles would be enhanced at the high-over maturity stages, which would also influence the measured reflectance results.

In a word, these optical reflectance parameters have unique application domains, and several external and internal factors influencing the accuracy of empirical equations for the $EqVR_o$ values should be taken into consideration, mainly including geological background of studied samples, measurement errors, and the option of different empirical equations. Moreover, greater artificial errors would be obvious in the over mature samples. In order to obtain accurate thermal maturity, different optical indicators can be adopted based on specific features of studied samples, and the measured data should be comprehensively analyzed.

4. Raman spectroscopy

4.1. Basic principle and Raman spectral parameters

Raman spectroscopy can be categorized as a technique characterizing the structure of molecules based on the Raman scattering, and the shift and intensity of characteristic peaks can directly reflect the vibrational modes of molecules and crystals

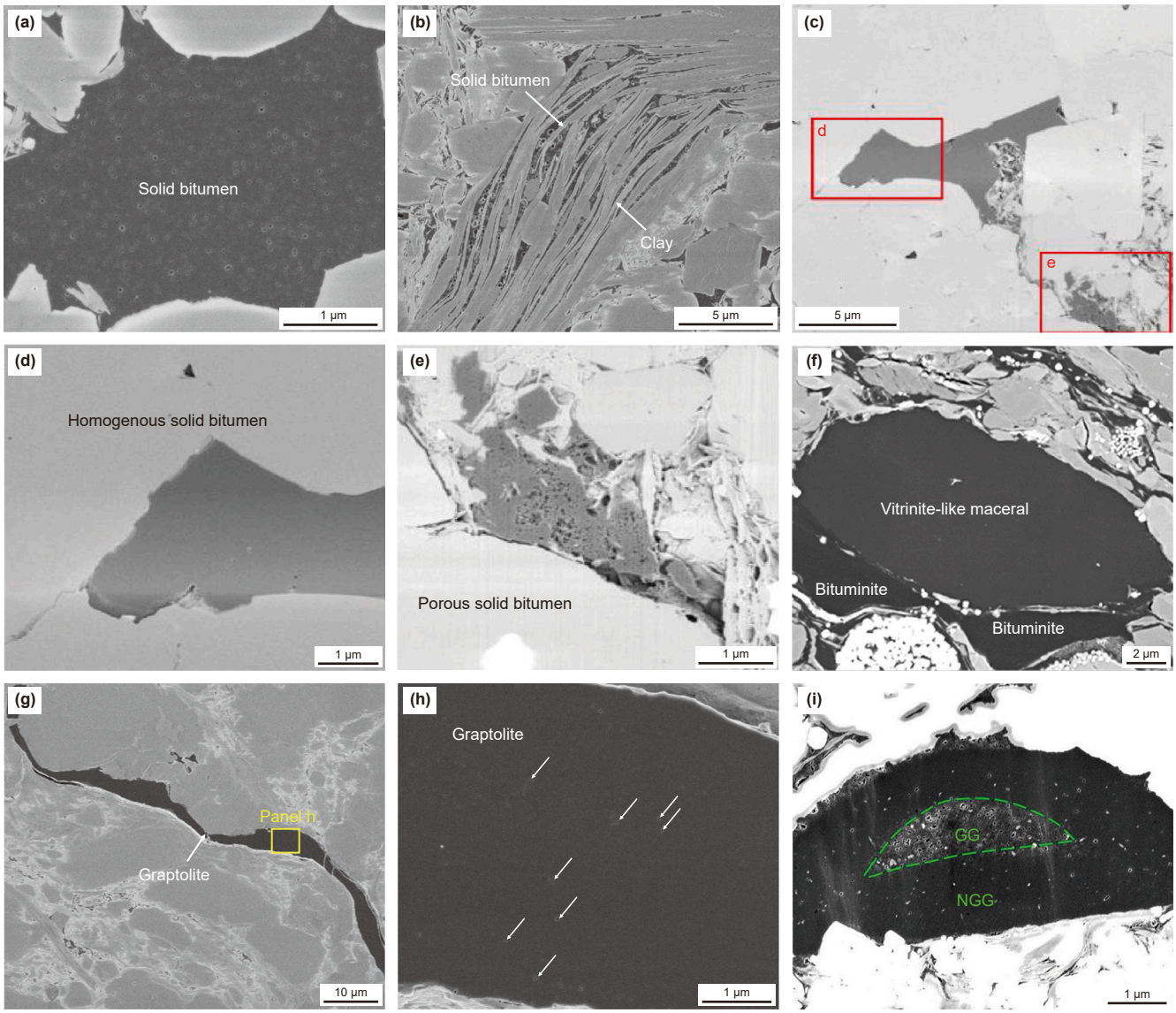

Fig. 7. SEM photographs showing pore characteristics of the SB and graptolite particles. **(a)** SEM photograph showing an amorphous SB particle hosting numerous pores occupied within the intergranular pores of minerals in the WF-LMX black shale. **(b)** SEM photograph showing the SB particles hosting numerous pores distributed among clay platelets in the WF-LMX black shale. **(c–e)** BSE photograph showing different SB with little nanopore (d) and the SB with abundant nanopores (e) in the tight gas siltstone sample from the Montney Formation (Sanei et al., 2015). **(f)** SEM photograph showing the VLM displaying a clear boundary with bituminite, and the bituminite fill the space between mineral grains (Luo et al., 2021). **(g)** SEM photograph showing an elongated graptolite particle in the WF-LMX black shale. **(h)** A close-up image delineated by the yellow rectangle in Fig. (g) illustrating few SEM-visible pores in the graptolite in the WF-LMX black shale. **(i)** SEM photograph showing a transect graptolite displaying different pore characteristics of different parts of graptolite, including porous in the interior and less porous or no pores in the rim (Zheng et al., 2022).

hosted in the materials, providing the detailed information on chemical compositions of the materials and crystal configuration features (Yui et al., 1996). In the material science, Raman spectroscopy has been used to determine the average domain size of graphitic crystallites in carbonaceous materials (Kelemen and Fang, 2001). In the field of geoscience, Raman spectroscopy has been increasingly used to determine the thermal alteration of OM as a result of rapid and non-destructive measurements (Henry et al., 2019b; Khatibi et al., 2019; Liu et al., 2013; Sauerer et al., 2017; Schito et al., 2017; Wilkins et al., 2015). During thermal maturation, chemical compositions and structures of sedimentary OM could be irreversibly altered, and progressive exhaustion of hydrogen atoms and heteroatomic groups would lead to a transformation of molecular structures from disorder to order, which can be identified by the Raman spectrum (Beyssac and Rumble, 2014; Ferralis et al., 2016; Henry et al., 2019a, 2019b; Schito et al., 2017, 2023). Numerous studies have also proved that Raman spectroscopy is a useful geothermometer for geological samples, including kerogen, bitumen, graptolite, and other carbonaceous materials (Hao et al., 2019; Kelemen and Fang, 2001; Meng et al., 2022; Schmidt and İnan, 2016; Song et al., 2023; Zhou et al., 2014).

Raman spectrum of the OM is mainly composed of two regions, including first-order region (1000–1800 cm^{-1}) and second-order region (2400–3500 cm^{-1}) (Fig. 8(a)–(c)) (Tuinstra and Koenig, 1970). The first-order region comprises the D-band (disordered peak) and the G-band (ordered peak or graphite peak) (Fig. 8(a) and (b)). D-band, also known as A-band or D1-band, occurs at the Raman shift of 1250–1450 cm^{-1}, which is related to the breathing motion of the sp^2 atoms in an aromatic ring having a A_{1g} symmetry

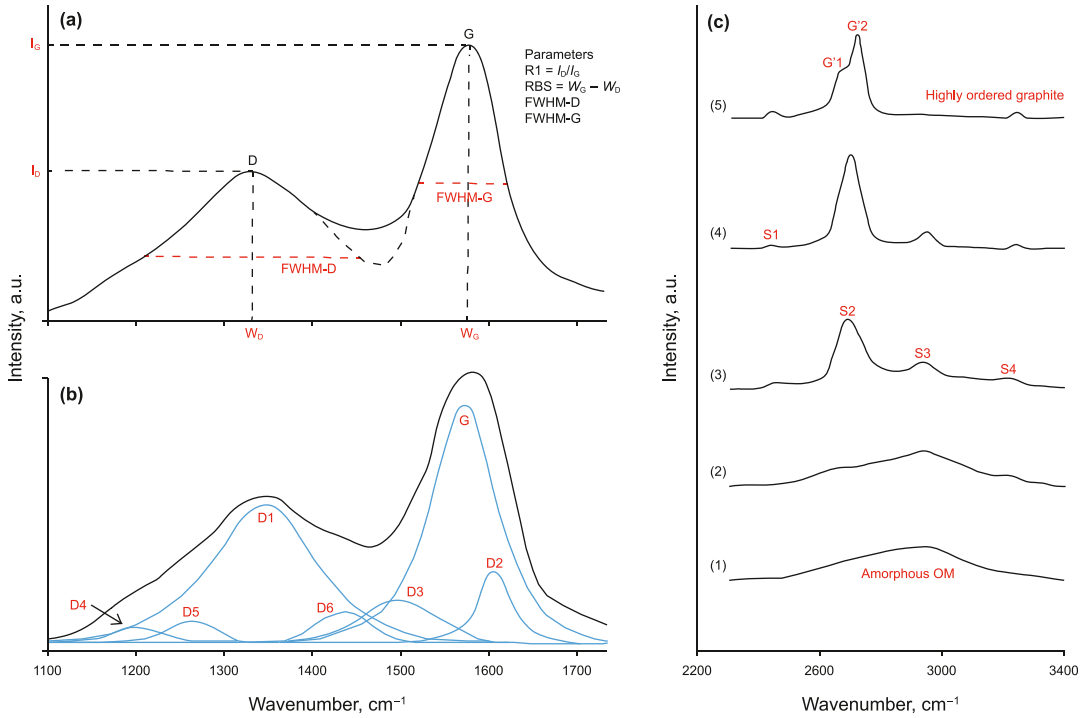

Fig. 8. **(a)** Non-deconvolved Raman spectrum showing first-order Raman bands of OM and Raman parameters that can be calculated, including W_D, W_G, FWHM-D, FWHM-G, RBS and I_D/I_G ($R1$). **(b)** 6-band deconvoluted spectrum with the proposed nomenclature of the bands when performing deconvolution. **(c)** A diagram showing the variation of second-order Raman bands of OM with increasing maturity (ordering). (1–2) amorphous OM. (3–4) ordered graphite. (5) highly ordered graphite. All figures were modified from Henry et al. (2019a).

mode vibration (Tuinstra and Koenig, 1970). The G-band, located in the Raman shift of 1500–1650 cm^{-1}, is related to the in-plane vibration of carbon atoms in graphene sheets with E_2g_2 symmetry, which is the in-plane vibration of carbon atoms in graphene sheets (Liu et al., 2013; Pimenta et al., 2007; Reich and Thomsen, 2004; Tuinstra and Koenig, 1970). It has been previously reported that the intensity of D-band would be lowered and the width of G-band would be decreased with increasing maturity (Xiao et al., 2020). Therefore, many Raman spectral parameters are commonly used as effective indicators to assess organic maturity of sediments (Guedes et al., 2010; Hao et al., 2019; Liu et al., 2013; Marques et al., 2009; Sauerer et al., 2017).

The second-order region appears as a broad band at low maturity stages and separates into several obvious and identifiable bands at the anthracite stage, e.g., S1 (2450 cm^{-1}), S2 (2700 cm^{-1}), S3 (2950 cm^{-1}) and S4 (3200 cm^{-1}) (Fig. 8(c)) (Beyssac et al., 2002; Liu et al., 2013; Pasteris and Wopenka, 1991; Wang et al., 2019). With the beginning of OM graphitization, the S2 and S3 peaks become clearer and the S1 peak becomes visible (Fig. 8(c)). With the increasing degree of graphitization, the intensity of S2-band is gradually increasing and the intensities of S1, S3 and S4 bands are decreasing. Subsequently, the S2 peak would be gradually split apart to G1' and G2' peaks in highly-ordered graphite (Beyssac et al., 2002; Henry et al., 2019a; Lespade et al., 1982; Rantitsch et al., 2016). In addition, the S3 peak shows systematic peak shifting toward higher wavenumbers with the increasing R_o values, indicating that S3 peak position may be a potential maturity indicator (Spötl et al., 1998; Wang et al., 2021). At present, the formation of second-order bands has been widely attributed to a mixture of overtones and combinations of distinct inelastic scattering of the bands in the first-order region (Beyssac et al., 2002; Childress and Jacobsen, 2017; Wopenka and Pasteris, 1993), but further investigation is required.

4.2. Raman maturity indicators and their relationships with reflectance of different macerals

Beny-Bassez and Rouzaud (1985) firstly found that the Raman spectroscopy could be used for evaluating the OM coalification and graphitization degree based on artificially heated samples. Subsequently, Spötl et al. (1998) demonstrated that the Raman spectroscopy can be used to determine the VR_o values within a large maturity range of 0.38%–6.1% based on a series of naturally-matured samples. Wilkins et al. (2014, 2015) proposed that the Raman Maturity Method (RaMM) was a non-graphical technique for thermal maturity determination covering the VR_o range of 0.4%–2.5%. Numerous authors have also found the close links between first-order vibrational bands and the maturity degree of the measured OM, and the width and height, relative intensity ratio, and position changes for the D-band and G-band can be quantitatively indicated by different parameters, including the position of the D-band (W_D) and G-band (W_G), Raman band separation (RBS), the full width at maximum height of D-band and G-band (FWHM-D, FWHM-G), and the intensity ratio of D and G bands ($R1$ or I_D/I_G) and so on (Table 5; Beyssac et al., 2002; Henry et al., 2019a, 2019b; Kelemen and Fang, 2001; Liu et al., 2013; Meng et al., 2024; Sauerer et al., 2017; Schito et al., 2016, 2017; Wilkins et al., 2014, 2015).

A large number of the naturally and artificially maturated samples has revealed systematic changes between several Raman parameters and maturity levels, but there still have some differences on the variation tendencies of the Raman parameters (Fig. 9). At the low maturity stage, strong fluorescence interferences are often present in the Raman spectrum (Schmidt and İnan, 2016). Additionally, the D-band displays irregular morphology and lower intensities, and only the G-band shows the relatively clear morphology (Beyssac et al., 2002; Ferralis et al.,

Table 5
The empirical equations for equivalent vitrinite reflectance calculation ($EqVR_o$, %) based on Raman spectroscopy parameters.

Empirical equations	Applicable conditions	Materials/age/area	References
$\lg(X_{1600}) = -0.0720EqVR_o+5.5256$ $\lg(X_{1350}) = -0.1147EqVR_o+6.0076$ $\ln(Y) = 0.0985EqVR_o-1.0930$ $\ln(RBS) = -0.0582\ln(EqVR_o)+5.5834$	2.1% < $EqVR_o$ < 15.0%	Paleogene sedimentary rocks and metamorphic rocks in the Australia	Wang and Hu (2002)
$EqVR_o = 0.0537RBS-11.21$ $EqVR_o = 1.1659I_D/I_G+2.7588$	Medium-high mature Overmature-ex-graphite	Standard coal and solid OM samples of varying maturity levels	Liu et al. (2013)
$EqVR_o = -6.384 + 5.429\log(RBS)+0.863\log('b') +0.832\log$ (saddle index)$-2.677\log$(FWHM-G)$-0.611\log$(FWHM-D)	0.4% < $EqVR_o$ < 1.2%	Reference coal samples from the Joint Coal Board Evaluation Laboratory, Cessnock, NSW	Wilkins et al. (2014)
$EqVR_o = -52.3363 + 13.1992\log(RBS)-0.7964\log('b')+8.1121\log$ (FWHM-D)$+15.3255\log(I_D/I_G)$	1.0% < $EqVR_o$ < 2.5%	Permian coals in the northern Carnarvon Basin of Western Australia	Wilkins et al. (2015)
$EqVR_o = 0.089RBS-19.937$	Graptolite-bearing shales	Ordovician-Silurian shale samples from Sichuan Basin and Ordovician Alum Shales from Sweden and Estonia	Hao et al. (2019)
$EqVR_o = 0.030RBS-5.538$	0.4% < $EqVR_o$ < 3.35%	Abitibi shale, Ordovician–Silurian shale and coal samples, data from Birdwell and Wilson (2019), Hackley et al. (2020), Stefanopoulos et al. (2017), Ruppert et al. (2013), Lupoi et al. (2019) and Tewalt et al. (2010)	Stokes et al. (2023)

Note: X_{1600}, X_{1350} refer to the peak areas of the G-band and D-band, respectively. Y refers to the area ratio of the D-band and G-band. 'b' refers to the slope of the linear spectral background. Saddle index refers to the height ratio of the G-band to the minimum of the saddle between the overlapping G-band and D-band.

2016). With the increasing maturity levels, the D-band and G-band display more notable morphologies (Henry et al., 2019b). The positions of two bands are close to each other, and area ratio of two peaks gradually increases (Ferralis et al., 2016). In addition, second-order vibrational peaks can be appeared within the Raman shift of 2500–2700 cm^{-1} at the VR_o > 2.0% stage (Fig. 8(c)) (Beyssac et al., 2002; Liu et al., 2013; Pasteris and Wopenka, 1991; Xiao et al., 2020; Wang et al., 2019).

Although the absolute values of the Raman parameters from previous studies are very hard to be compared due to the various deconvolution methods and experiment conditions, some trends between the Raman parameters and optical reflectance values can be clearly described for various OM particles (Fig. 9). Firstly, the W_D and W_G values would be changed to some extents with the increasing maturity levels (Fig. 9(a) and (b)). The W_D values show an overall decreasing trend, but display a reverse trend at the over mature stages with a "turning point" at 3.5%–4.0% VR_o (Fig. 9(a)), indicating the transformation of disordered carbon to ordered graphite (Hou et al., 2019). However, the W_G values seem to display an overall slight increase trend (Fig. 9(b)), indicating the increasing abundance of aromatic compounds and enhanced polycyclicity (Schmidt and İnan, 2016). In fact, the position of G-band may be shifted due to the related variation of the single/double bond strength of aromatic rings and chains (Schmidt and İnan, 2016). Thus, this scenario could be resulted from the transformation and reduction of amorphous carbon, as well as the rapid increase of aromatic sheets during thermal maturation (Wang et al., 2023).

The RBS values show a nonlinear relationship with optical reflectance values (Fig. 9(c)). At the VR_o values less than 3.5%–4.0%, a rapid rise of the RBS values can be observed, while the trend becomes a flat or slightly decreased pattern when the VR_o values more than 3.5%–4.0% (Fig. 9(c)). The observed increase of the RBS values at the first stage may be resulted from the decreasing quantity of disordered carbon in the OM. However, a slight decrease of the RBS values at the second stage may be related to the increasing aromaticity of the OM, since a portion of aliphatic side chains would be dropped among aromatic rings during the condensation and polymerization of aromatic components at the higher maturity stages (Hao et al., 2019; Henry et al., 2019a, 2019b; Liu et al., 2013; Sauerer et al., 2017; Wang et al., 2023; Xiao et al., 2020; Zhou et al., 2014).

The widths of the D-band and G-band were principally suggested to be a function of crystallite size as well as degree of defects (Dillon and Woollam, 1984). At the lower VR_o values, the larger width of D-band indicates the presence of the chars containing aromatic rings of various sizes, but graphite crystals are impossible to be formed (Li et al., 2006). With the increasing maturity levels, the morphology of G-band and D-band would become sharper and narrower, displaying a sharp decrease of the FWHM-D values (Fig. 9(d)). However, the FWHM-D values display the dichotomous trends with the increasing VR_o values, which represent disparate patterns in naturally and artificially matured samples, respectively (Fig. 9(d)). Some authors have revealed that Raman spectra data showed different maturation rates between naturally- and artificially-matured samples, indicating the as yet undetermined differences in carbon chemistry. The considerable differences between naturally- and artificially-matured samples may be attributed to different structural information captured by Raman and reflectance measurements, and to the incomplete structural transformation of artificially matured samples. (Hackley and Lünsdorf, 2018; Khatibi et al., 2019; Hao et al., 2019). In contrast, the FWHM-G values display an overall slow decreasing tendency with the increasing maturity, and an opposite tendency occurred at the VR_o > 3.5%–4.0% (Fig. 9(e)), probably resulting from the transformation of amorphous carbon to crystalline graphite within the kerogen (Kouketsu et al., 2014; Wang et al., 2023).

Yui et al. (1996) suggested that the height of the Raman peaks could not indicate any physical meaning, but the variation trend of the I_D/I_G ratio (termed as $R1$) represented the decoupling of the changing rate of increase in both in-plane crystallite size and degree of defects in carbonaceous materials during progressive metamorphism. However, some authors believed that the I_D/I_G ratio represented the ordering degree of internal molecular structure of OM (Zhang and Li, 2019; Zhou et al., 2014). The I_D/I_G ratio displays no significant variations or an overall slight decreasing tendency with the increasing maturity at the VR_o < 3.5%–4.0% (Fig. 9(f)), implying the slow growth of aromatic rings within the OM. The chemical structure of the OM is transitioning from amorphous carbon to crystalline graphite (Wang et al., 2019), thus resulting in the formation of larger conjugated aromatic clusters having the decreased amounts of aliphatic chains and higher structural ordering degrees (Du et al., 2014). At the VR_o >

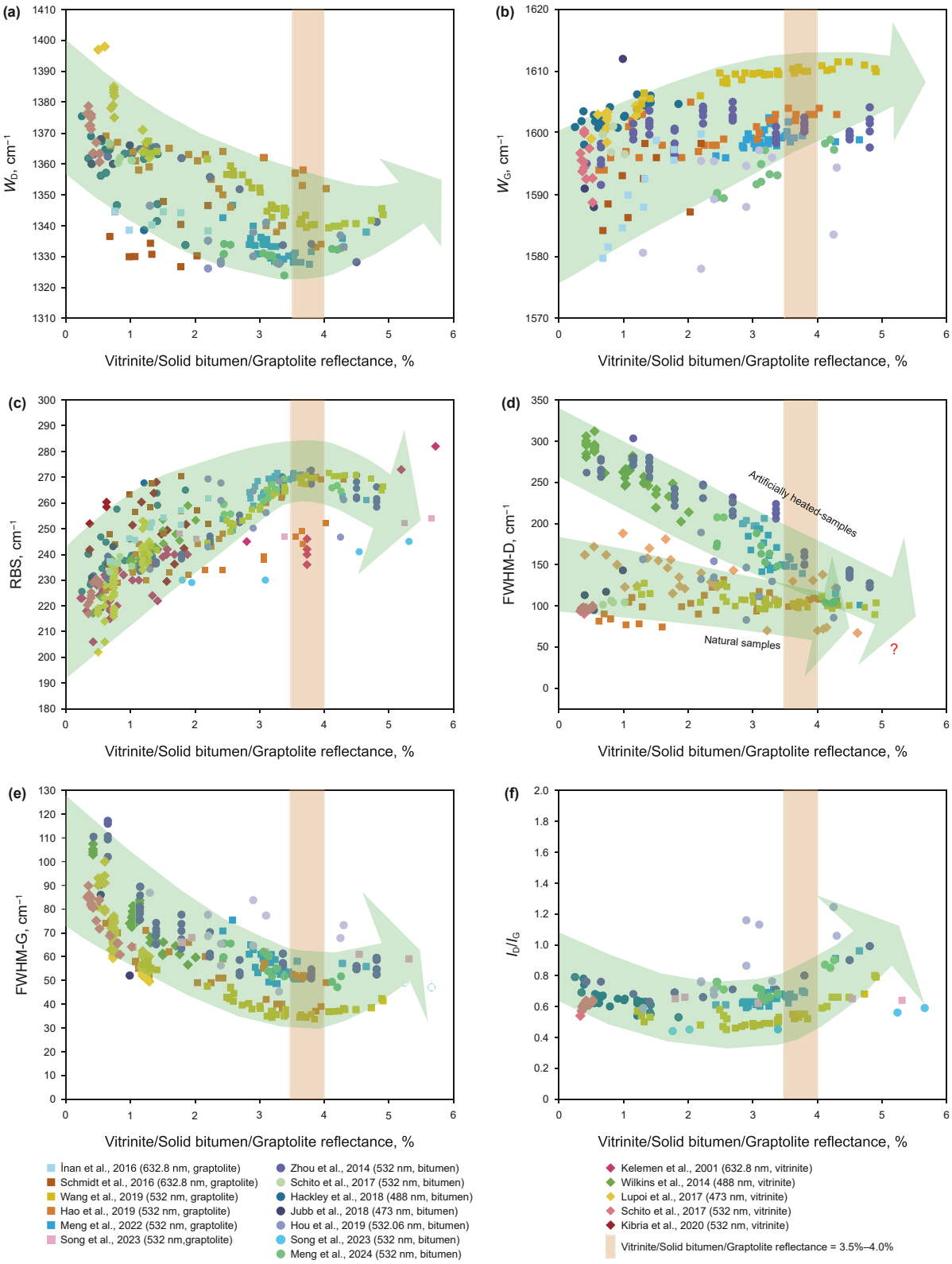

Fig. 9. The relationships between Raman parameters and optical reflectance for different macerals sourced from previous studies, illustrating the general trend of parameter evolution with increasing reflectance. **(a)** D-band position. **(b)** G-band position. **(c)** RBS. **(d)** FWHM-D. **(e)** FWHM-G. **(f)** I_D/I_G. Data are from Hackley et al. (2018), Hao et al. (2019), Hou et al. (2019), İnan et al. (2016), Jubb et al. (2018), Kelemen and Fang (2001), Kibria et al. (2020), Lupoi et al. (2019), Meng et al. (2022, 2024), Schito et al. (2017), Schmidt and İnan (2016), Song et al. (2023), Wang et al. (2019), Wilkins et al. (2014), Zhou et al. (2014).

3.5%–4.0%, the I_D/I_G ratio shows a significant increasing tendency (Fig. 9(f)), suggesting a rapid increase of aromatic clusters within the OM (Wang et al., 2023).

In summary, the FWHM-G and RBS values can be regarded as the highly reliable indicators for assessing thermal maturity of source rocks at various maturity stages, but they cannot indicate the matuirty levels within the VR_o range of 3.5%–4.0%. The I_D/I_G ratio can be used for an effective maturity indicator at the VR_o > 3.5%. The relationships between other Raman parameters and optical reflectance values have not been established yet, which are largely accounted for the significant effect of different data processing methods on the calculated Raman parameters.

4.3. Advantages and limitations

Raman spectroscopy is increasingly becoming an alternative approach to determine thermal maturity of the OM, directly reflecting the molecular structure of OM (Henry et al., 2019a). The advantages of the Raman technique mainly include in the following two aspects. (1) Raman spectrometry is a rapid and non-destructive approach to evaluate thermal maturity, and the analytical spot size is generally only a few microns (Schmidt and İnan, 2016). For the measurement of powdered samples, only small amounts of samples (dozens of mg) are needed (e.g., Zhou et al., 2014). Recently, Xiao et al. (2020) also suggested that the Raman technique was very sensitive to the OM in mineral-organic aggregations (MOA), and found that perfect Raman spectra with D-band and G-band derived from the OM in the MOA could be obtained when the TOC content of studied shale samples reached about 0.6%. Moreover, the Raman parameters of the MOA were in good agreement with those of the associated SB (Xiao et al., 2020), indicating that the Raman spectrometry could be used as a potential tool to assess thermal maturity of low-TOC source rocks. (2) The dispersion degree of measured Raman parameters is relatively low relative to optical reflectance parameters. Moreover, the identification of different macerals and optical anisotropy can be neglected during the measurement of Raman spectroscopy, which must be taken into consideration during optical reflectance measurement (Liu et al., 2013). For example, Liu et al. (2013) found that the Raman parameters of different macerals and SB particles displaying strong optical anisotropies at the high-over mature stages tended to be similar characteristics, indicating that Raman spectroscopy could be widely used for assessing thermal maturity of highly-matured shale samples and have huge prospects in geological applications. Recently, Zuo et al. (2022b) also found that the reservoir SB displaying different optical textures shared the same graphite crystal defects and sizes, and surface roughness cannot affect the Raman parameters.

Although the Raman spectroscopy offers several advantages, there still have some limitations on the application of such an approach in thermal maturity evaluation. (1) The standards of sample types, experimental conditions and curve fitting are lacked (Beyssac et al., 2002; Henry et al., 2019a; Sauerer et al., 2017; Wilkins et al., 2014; Xiao et al., 2020). The Raman spectrum is subject to variation as a result of varying test conditions, including the laser wavelength, the laser power, the experimental temperature, and so forth (Henry et al., 2019b). It is widely acknowledged that distinct laser wavelengths could impact the D-band region of OM (Ferrari and Robertson, 2001; Henry et al., 2018; Sauerer et al., 2017; Vidano et al., 1981). The Raman shift of D-band would be increased with increasing excitation wavelength, whereas the position of G-band remains unaffected (Beyssac et al., 2002; Beyssac and Lazzeri, 2012; Jubb et al., 2018; Kouketsu et al., 2014). High laser power would lead the oxidization of measured OM particles due to the heating, thus resulting in the reduction of G-band position and the suppression of D-band intensity (Everall et al., 1991; Kagi et al., 1994). (2) It is widely accepted that sample types can affect the Raman spectrum (Ammar and Rouzaud, 2012; Beyssac et al., 2003; Henry et al., 2018; Lünsdorf, 2016). Until now, several sample types have been used for characterizing OM via Raman spectroscopy, including polished rock cut-surfaces, thin-sections, strew slides and rock chips (Beyssac et al., 2003; Henry et al., 2018; Lünsdorf, 2016; Schito et al., 2017; Wilkins et al., 2014). Previous authors have suggested that the polishing of rock surfaces would lead to the decrease of D-band position and the increase of D-band intensity due to the frictional heating (Henry et al., 2018; Lünsdorf, 2016). Additionally, it is rapid and economical to use the unpolished rock-chips for Raman analysis, but it may be challenging to locate OM particles under the microscope and avoid the fluorescence produced by adjacent minerals (Sauerer et al., 2017; Henry et al., 2019a). However, potential effects of sample types on the Raman spectrum remains unclear, and further work is needed to suggest an optimized sample preparation method for assessing the OM thermal maturity. (3) The deconvolution of Raman spectrum and the number of fitted peaks (2–10) in the first-order region are varied by different authors, and the Raman results of previous works are very hard to be compared (Henry et al., 2019b), thus hindering the extensive applications in case studies. Some authors suggested that a simple 2-band deconvolution, only including the D-band and G-band, may be more reliable for the wide utilization of Raman spectroscopy as a geothermometer (Xiao et al., 2020), since muli-band deconvolution methods may yield more artificial errors during the peak fitting.

5. Summary and prospects

Thermal maturity assessment is still challenging for the Precambrian–Lower Paleozoic high-over mature marine shale deposits due to the absence of vitrinite, hindering the evaluations of resource potentials of source rocks and gas-bearing properties of shale reservoirs. At present, optical reflectance indicators (e.g., SBR_o, $VLMR_o$ and GR_o) and Raman maturity indicators (e.g., FWHM-G, RBS and I_D/I_G) have been widely used for thermal maturity assessment, while these indicators have favorable application conditions and several limitations. This review systematically investigated the optical and Raman maturity indicators, and several conclusions can be drawn.

(1) According to the optical properties (reflectance, fluorescence) and structural features (e.g., morphology, texture) of organic materials, four types of macerals, i.e., solid bitumen, vitrinite-like maceral, zooclasts, and liptinite, can be identified in the Precambrian–Lower Paleozoic sedimentary rocks. Solid bitumen is secondary maceral formed from thermal degradation of kerogen or crude oils, and usually displays amorphous shapes filling in pores, voids, and cracks of rocks. Vitrinite-like maceral is a primary maceral that may be formed from the humification or strong bacterial degradation of marine lower organisms, displaying the rounded or lenticular-elongated shapes. Zooclasts mainly consist of graptolite, chitinozoan vesicle and radiolarian with distinct biological structures.

(2) Solid bitumen, vitrinite-like maceral and graptolite have been widely used for optical reflectance measurements. However, incorrect identification and optical characteristics of different macerals would lead to artificial errors during maturity evaluation, and various empirical equations for the $EqVR_o$ values based on different optical reflectance indicators display greater variations. According to large

amounts of measured points from previous works, two empirical equations for the $EqVR_o$ values have been established based on the SBR_o and $VLMR_o$ values, respectively, i.e., $EqVR_o = 0.71SBR_o+0.31$ ($R^2 = 0.99$), and $EqVR_o = 0.86VLMR_o+0.37$ ($R^2 = 0.93$). However, the universality and accuracy of the above two empirical equations remain to be examined, due to the limitations of selected data and different application conditions.

(3) Raman spectroscopy, with the characteristics of economical, rapid, non-destructive, and high-resolution measurements, provides an alternative approach to assess thermal maturity, which can be utilized independently or be complemented with other traditional maturity indicators. The FWHM-G and the RBS may be the most reliable parameters to assessing thermal maturity at the VR_o = 0.5%~3.5%–4.0%, while the I_D/I_G ratio may be the only reliable maturity parameter at the VR_o > 3.5%–4.0%. It is still challenging to indicate the maturity levels within the VR_o range of 3.5%–4.0% by using Raman parameters. In addition, a paucity of unified standards in those areas such as sample preparation, testing conditions, fitting equations, and peak fitting number, directly impacts the widespread use of the Raman spectroscopy in assessing thermal maturity.

(4) It is critical to realize that every indicator has both advantages and limitations. As for thermal maturity assessment of high-over mature shale reservoirs devoid of vitrinite, a variety of maturity indicators should be comprehensively used to yield accurate results. Among them, optical reflectance of SB has been widely used in many case studies, but cautions must be paid in accurate identification and optical anisotropy of SB particles, as well as the selection of empirical equations for the $EqVR_o$ values. Raman spectroscopy can be used as a complementary approach to assess thermal maturity. Therefore, optical reflectance and Raman spectroscopy should be jointly used in thermal maturity assessment of the Precambrian–Lower Paleozoic high-over mature shale reservoirs to yield more precise maturity information for shale gas exploration and development.

CRediT authorship contribution statement

Si-Yi Liu: Software, Data curation, Visualization, Writing – original draft, Investigation, Methodology. **Ping Gao:** Supervision, Conceptualization, Resources, Writing – review & editing, Project administration. **Xian-Ming Xiao:** Supervision, Resources, Conceptualization, Project administration. **Qin Zhou:** Project administration, Resources, Conceptualization. **Yan-Ming Zhao:** Data curation, Conceptualization. **Wei Liu:** Data curation, Conceptualization.

Declaration of competing interest

The authors declare that they have no known competing financial interests or personal relationships that could have appeared to influence the work reported in this paper.

Acknowledgements

This work was supported by the National Natural Science Foundation of China (42030804, 42272140, 42373051), the CNPC Innovation Fund (2022DQ02-0107), and the “Deep-time Digital Earth” Science and Technology Leading Talents Team Funds for the Central Universities for the Frontiers Science Center for Deep-time Digital Earth, China University of Geosciences (Fundamental Research Funds for the Central Universities, 2652023001).

Appendix

Abbreviations	Terminology
OM	Organic matter
GG	Granular graptolite
NGG	Non-granular graptolite
SBR_o	Solid bitumen reflectance
$VLMR_o$	Vitrinite-like maceral reflectance
$VLMR_{omax}$	Vitrinite-like maceral maximum reflectance
GR_o	Non-granular graptolite random reflectance
GR_{omax}	Non-granular graptolite maximum reflectance
VR_o	Vitrinite reflectance
$EqVR_o$	Equivalent vitrinite reflectance
W_D	The Raman shift of D-band
W_G	The Raman shift of G-band
FWHM-D	Full width at half maximum of D-band
FWHM-G	Full width at half maximum of G-band
RBS	Raman band separation
I_D/I_G	Raman band height ratio of D-band and G-band

References

Abraham, H., 1918. Asphalts and Allied Substances, Their Occurrence, Modes of Production, Uses in the Arts and Methods of Testing. D. Van Nostrand Company, Inc., New York.

Agirrezabala, L.M., Permanyer, A., Suárez-Ruiz, I., Dorronsoro, C., 2014. Contact metamorphism of organic-rich mudstones and carbon release around a magmatic sill in the Basque-Cantabrian Basin, western Pyrenees. Org. Geochem. 69, 26–35. https://doi.org/10.1016/j.orggeochem.2014.01.014.

Ai, J.Y., Zhong, N.N., Zhang, T.G., Zhang, Y., Wang, T.G., George, S.C., 2021. Oceanic water chemistry evolution and its implications for post-glacial black shale formation: Insights from the Cryogenian Datangpo Formation, South China. Chem. Geol. 566, 120083. https://doi.org/10.1016/j.chemgeo.2021.120083.

Ammar, M., Rouzaud, J.N., 2012. How to obtain a reliable structural characterization of polished graphitized carbons by Raman microspectroscopy. J. Raman Spectrosc. 43 (2), 207–211. https://doi.org/10.1002/jrs.3014.

Araujo, C.V., Borrego, A.G., Cardott, B., et al., 2014. Petrographic maturity parameters of a Devonian shale maturation series, Appalachian Basin, USA. ICCP Thermal Indices Working Group interlaboratory exercise. Int. J. Coal Geol. 130, 89–101. https://doi.org/10.1016/j.coal.2014.05.002.

Ardakani, O.H., Sanei, H., Ghanizadeh, A., Lavoie, D., Chen, Z.H., Clarkson, C.R., 2018. Do all fractions of organic matter contribute equally in shale porosity? A case study from Upper Ordovician Utica Shale, southern Quebec, Canada. Mar. Petrol. Geol. 92, 794–808. https://doi.org/10.1016/j.marpetgeo.2017.12.009.

Beny-Bassez, C., Rouzaud, J.N., 1985. Characterization of carbonaceous materials by correlated electron and optical microscopy and Raman microspectroscopy. Scan. Electron. Microsc. 1, 119–132.

Bernard, S., Horsfield, B., 2014. Thermal maturation of gas shale systems. Annu. Rev. Earth Planet Sci. 42, 635–651. https://doi.org/10.1146/annurev-earth-060313-054850.

Bernard, S., Horsfield, B., Schulz, H.-M., Wirth, R., Schreiber, A., Sherwood, N., 2012a. Geochemical evolution of organic-rich shales with increasing maturity: a STXM and TEM study of the Posidonia Shale (Lower Toarcian, northern Germany). Mar. Petrol. Geol. 31 (1), 70–89. https://doi.org/10.1016/j.marpetgeo.2011.05.010.

Bernard, S., Wirth, R., Schreiber, A., Schulz, H.-M., Horsfield, B., 2012b. Formation of nanoporous pyrobitumen residues during maturation of the Barnett shale (Fort Worth Basin). Int. J. Coal Geol. 103 (23), 3–11.

Bertrand, R., 1990. Correlations among the reflectances of vitrinite, chitinozoans, graptolites and scolecodonts. Org. Geochem. 15 (6), 565–574. https://doi.org/10.1016/0146-6380(90)90102-6.

Bertrand, R., 1993. Standardization of solid bitumen reflectance to vitrinite in some Paleozoic sequences of Canada. Energy Sourc. 15 (2), 269–287. https://doi.org/10.1080/00908319308909027.

Bertrand, R., Malo, M., 2001. Source rock analysis, thermal maturation and hydrocarbon generation in Siluro-Devonian rocks of the Gaspé Belt basin, Canada. Bull. Can. Petrol. Geol. 49, 238–261. https://doi.org/10.2113/49.2.238.

Bertrand, R., Malo, M., 2012. Dispersed organic matter reflectance and thermal maturation in four hydrocarbon exploration wells in the Hudson Bay Basin: Regional implications. Geolog. Surv. Canada Open File 7066, 1–25.

Bertrand, R., Lavoie, D., Fowler, M., 2003. Cambrian–Ordovician shales in the Humber zone: Thermal maturation and source rock potential. Bull. Can. Petrol. Geol. 51, 213–233. https://doi.org/10.2113/51.3.213.

Beyssac, O., Goffé, B., Chopin, C., Rouzaud, J.N., 2002. Raman spectra of carbonaceous material in metasediments: A new geothermometer. J. Metamorph. Geol. 20, 859–871. https://doi.org/10.1046/j.1525-1314.2002.00408.x.
Beyssac, O., Goffé, B., Petitet, J.P., Froigneux, E., Moreau, M., Rouzaud, J.N., 2003. On the characterization of disordered and heterogeneous carbonaceous materials by Raman spectroscopy. Spectrochim. Acta, Part A 59 (10), 2267–2276. https://doi.org/10.1016/S1386-1425(03)00070-2.
Beyssac, O., Lazzeri, M., 2012. Application of Raman spectroscopy to the study of graphitic carbons in the Earth science. EMU Note. Mineral. 12 (12), 415–454. https://doi.org/10.1180/EMU-notes.12.12.
Beyssac, O., Rumble, D., 2014. Graphitic carbon: A ubiquitous, diverse, and useful geomaterial. Elements 10 (6), 415–420. https://doi.org/10.2113/gselements.10.6.415.
Birdwell, J.E., Wilson, S.A., 2019. Variability in results from mineralogical and organic geochemical Interlaboratory Testing of U. S. Geological survey Shale reference materials. Unconvent. Resourc. Technol. Conf. 457, 1–19.
Borjigin, T., Lu, L.F., Yu, L.J., Zhang, W.T., Pan, A.Y., Shen, B.J., Wang, Y., Yang, Y.F., Gao, Z.W., 2021. Formation, preservation and connectivity control of organic pores in shale. Petrol. Explor. Dev. 48 (4), 687–699. https://doi.org/10.11698/PED.2021.04.02 (in Chinese).
Buchardt, B., Lewan, M.D., 1990. Reflectance of vitrinite-like macerals as a thermal maturity index for Cambrian–Ordovician Alum Shale, southern Scandinavia. AAPG Bull. 74, 394–406.
Buseck, P.R., Beyssac, O., 2014. From organic matter to graphite: Graphitization. Elements 10 (6), 421–426. https://doi.org/10.2113/gselements.10.6.421.
Bustin, R., Link, C., Goodarzi, F., 1989. Optical properties and chemistry of graptolite periderm following laboratory simulated maturation. Org. Geochem. 14, 355–364. https://doi.org/10.1016/0146-6380(89)90001-6.
Cao, Y., Han, H., Liu, H.W., Jia, J.C., Zhang, W., Liu, P.W., Ding, Z.G., Chen, S.J., Lu, J.G., Gao, Y., 2019. Influence of solvents on pore structure and methane adsorption capacity of lacustrine shales: An example from a Chang 7 shale sample in the Ordos Basin, China. J. Pet. Sci. Eng. 178, 419–428. https://doi.org/10.1016/j.petrol.2019.03.052.
Cao, Y., Han, H., Guo, C., Pang, P., Ding, Z.G., Gao, Y., 2020. Influence of extractable organic matters on pore structure and its evolution of Chang 7 member shales in the Ordos Basin, China: Implications from extractions using various solvents. J. Nat. Gas Sci. Eng. 79, 103370. https://doi.org/10.1016/j.jngse.2020.103370.
Cao, C.Q., Shang, Q.H., Fang, Y.T., 2000. The study of graptolite reflectance as the indicator of source-rock maturation in Ordovician and Silurian of Tarim Basin, Ordos, Jiangsu areas. Acta Palaeontol. Sin. 39, 155–157 (in Chinese).
Cardott, B.J., Curtis, M.E., 2018. Identification and nanoporosity of macerals in coal by scanning electron microscopy. Int. J. Coal Geol. 190, 205–217. https://doi.org/10.1016/j.coal.2017.07.003.
Cardott, B.J., Landis, C.R., Curtis, M.E., 2015. Post-oil solid bitumen network in the Woodford Shale, USA—A potential primary migration pathway. Int. J. Coal Geol. 139, 106–113. https://doi.org/10.1016/j.coal.2014.08.012.
Cheng, D.S., Hao, S.S., Wang, F.Y., 1995. Reflectance of vitrinite-like macerals, a possible thermal maturity index for highly over-matured source rocks of the Lower Paleozoic. Petrol. Explor. Dev. 1, 25–28 (in Chinese).
Childress, L.B., Jacobsen, S.D., 2017. High-pressure high-temperature Raman spectroscopy of kerogen: Relevance to subducted organic carbon. Am. Mineral. 102, 391–403. https://doi.org/10.2138/am-2017-5719.
Clarkson, E.N.K., 1981. Invertebrate Paleontology and Evolution. George Allen & Unwin, Boston.
Crick, I.H., 1992. Petrological and maturation characteristics of organic matter from the Middle Proterozoic McArthur Basin, Australia. Aust. J. Earth Sci. 39, 501–519. https://doi.org/10.1080/08120099208728042.
Crick, I.H., Boreham, C.J., Cook, A.C., Powell, T.G., 1988. Petroleum geology and geochemistry of Middle Proterozoic McArthur Basin, northern Australia II: assessment of source rock potential. AAPG Bull. 72, 1495–1514.
Crowther, P.R., 1981. The fine structure of graptolite periderm. Spec. Pap. Palaeontol. (26) Palaeontological Association, London.
Curiale, J.A., 1986. Origin of solid bitumens, with emphasis on biological marker results. Org. Geochem. 10 (1/2/3), 559–580. https://doi.org/10.1016/0146-6380(86)90054-9.
Curtis, M.E., Cardott, B.J., Sondergeld, C.H., Rai, C.S., 2012. Development of organic porosity in the Woodford Shale with increasing thermal maturity. Int. J. Coal Geol. 103, 26–31. https://doi.org/10.2118/160158-MS.
De Wever, P., Dumitrica, P., Caulet, J.P., et al., 2002. Radiolarians in the Sedimentary Record. CRC Press.
Dillon, R., Woollam, J.A., 1984. Use of Raman scattering to investigate disorder and crystallite formation in AS-deposited and annealed carbon films. Carbon 22, 220. https://doi.org/10.1103/PhysRevB.29.3482, 220.
Du, J.Y., Geng, A.S., Liao, Z.W., Cheng, B., 2014. Potential Raman parameters to assess the thermal evolution of kerogens from different pyrolysis experiments. J. Anal. Appl. Pyrolysis 107, 242–249. https://doi.org/10.1016/j.jaap.2014.03.007.
Dutta, S., Hartkopf-Fröder, C., Witte, K., Brocke, R., Mann, U., 2013. Molecular characterization of fossil palynomorphs by transmission micro-FTIR spectroscopy: Implications for hydrocarbon source evaluation. Int. J. Coal Geol. 115, 13–23. https://doi.org/10.1016/j.coal.2013.04.003.
Endo, S., Wallis, S.R., Tsuboi, M., Torres De León, R., Solari, L.A., 2012. Metamorphic evolution of lawsonite eclogites from the southern Motagua fault zone, Guatemala: Insights from phase equilibria and Raman spectroscopy. J. Metamorph. Geol. 30 (2), 143–164. https://doi.org/10.1111/j.1525-1314.2011.00960.x.
Everall, N., Lumsdon, J., Christopher, D., 1991. The effect of laser-induced heating upon the vibrational Raman spectra of graphites and carbon fibres. Carbon 29 (2), 133–137. https://doi.org/10.1016/0008-6223(91)90064-P.
Feng, G.X., Chen, S.J., 1988. Relationship between bitumen reflectance and vitrinite reflectance in rocks. Nat. Gas. Ind. 8 (3), 20–25 (in Chinese).
Ferralis, N., Matys, E.D., Knoll, A.H., Hallmann, C., Summons, R.E., 2016. Rapid, direct and non-destructive assessment of fossil organic matter via microRaman spectroscopy. Carbon 108, 440–449. https://doi.org/10.1016/j.carbon.2016.07.039.
Ferrari, A.C., Robertson, J., 2001. Resonant Raman spectroscopy of disordered, amorphous, and diamondlike carbon. Phys. Rev. B 64 (7), 075414. https://doi.org/10.1103/PhysRevB.64.075414.
Gao, P., Liu, G.D., Lash, G.G., Li, B.Y., Yan, D.T., Chen, C., 2018. Occurrences and origin of reservoir solid bitumen in Sinian Dengying Formation dolomites of the Sichuan Basin, SW China. Int. J. Coal Geol. 200, 135–152. https://doi.org/10.1016/j.coal.2018.11.001.
Gao, P., Xiao, X.M., Hu, D.F., Lash, G.G., Liu, R.B., Cai, Y.D., Wang, Z.H., Zhang, B.Y., Yuan, T., Liu, S.Y., 2022. Effect of silica diagenesis on porosity evolution of deep gas shale reservoir of the Lower Paleozoic Wufeng–Longmaxi formations, Sichuan Basin. Mar. Petrol. Geol. 145, 105873. https://doi.org/10.1016/j.marpetgeo.2022.105873.
Gao, P., Xiao, X.M., Hu, D.F., Lash, G.G., Liu, R.B., Zhang, B.Y., Zhao, Y.M., 2024. Comparison of silica diagenesis between the lower Cambrian and lower Silurian shale reservoirs in the middle–upper Yangtze platform (Southern China). AAPG Bull. 108, 971–1003. https://doi.org/10.1306/01242422096.
Gentzis, T., Freitas, T.D., Goodarzi, F., Melchin, M., Lenz, A., 1996. Thermal maturity of Lower Paleozoic sedimentary successions in arctic Canada. AAPG Bull. 80, 1065–1084. https://doi.org/10.1306/64ED8C96-1724-11D7-8645000102C1865D.
Gentzis, T., Goodarzi, F., 1990. A review of the use of bitumen reflectance in hydrocarbon exploration with examples from Melville Island, Arctic Canada. Rocky Mountain Section (SEPM).
Goodarzi, F., 1984. Organic petrography of graptolite fragments from Turkey. Mar. Petrol. Geol. 1, 202–210. https://doi.org/10.1016/0264-8172(84)90146-6.
Goodarzi, F., Fowler, M., Bustin, M., McKirdy, D., 1992a. Thermal Maturity of Early Paleozoic Sediments as Determined by the Optical Properties of marine-derived Organic Matter—A Review, Early Organic Evolution. Springer, pp. 279–295. https://doi.org/10.1007/978-3-642-76884-2_21.
Goodarzi, F., Gentzis, T., Harrison, C., Thorsteinsson, R., 1992b. The significance of graptolite reflectance in regional thermal maturity studies, Queen Elizabeth Islands, Arctic Canada. Org. Geochem. 18, 347–357. https://doi.org/10.1016/0146-6380(92)90075-9.
Goodarzi, F., Gentzis, T., Luo, Q., Sanei, H., 2024. Bituminite–bitumen–migrabitumen. In: Borrego, A.G. (Ed.), The 75th ICCP Meeting. A Commemorative Book, pp. 109–123.
Goodarzi, F., Hosseininejad, S., Pedersen, P.K., Gentzis, T., Sanei, H., 2022. Characterization of immature oil shales from the Cretaceous Second White Specks Formation in Saskatchewan and Manitoba, Canada. Mar. Petrol. Geol. 143, 105774. https://doi.org/10.1016/j.marpetgeo.2022.105774.
Goodarzi, F., Macqueen, R., 1990. Optical/compositional character of six bitumen species from Middle Devonian rocks of the Pine point Pb-Zn property, Northwest Territories, Canada. Int. J. Coal Geol. 14 (3), 197–216. https://doi.org/10.1016/0166-5162(90)90003-H.
Goodarzi, F., Norford, B., 1985. Graptolites as indicators of the temperature histories of rocks. J. Geol. Soc. 142, 1089–1099. https://doi.org/10.1144/gsjgs.142.6.1089.
Goodarzi, F., Norford, B.S., 1989. Variation of graptolite reflectance with depth of burial. Int. J. Coal Geol. 11 (2), 127–141. https://doi.org/10.1016/0166-5162(89)90002-5.
Goodarzi, F., Snowdon, L.R., Gunther, P.R., Jenkins, W.A.M., 1985. Preliminary organic petrography of Palaeozoic rocks from the Grand Banks, Newfoundland. Mar. Petrol. Geol. 2 (3), 254–259. https://doi.org/10.1016/0264-8172(85)90015-7.
Grahn, Y., Paris, F., 2011. Emergence, biodiversification and extinction of the chitinozoan group. Geol. Mag. 148, 226–236. https://doi.org/10.1017/S0016756810000052X.
Guedes, A., Valentim, B., Prieto, A.C., Rodrigues, S., Noronha, F., 2010. Micro-Raman spectroscopy of collotelinite, fusinite and macrinite. Int. J. Coal Geol. 83, 415–422. https://doi.org/10.1016/j.coal.2010.06.002.
Hackley, P.C., Araujo, C.V., Borrego, A.G., Bouzinos, A., Cardott, B.J., Carvajal-Ortiz, H., López Cely, M.R., Chabalala, V., Crosdale, P., Demchuk, T.D., Eble, C.F., Furmann, A., Gentzis, T., Gonçalves, P.A., Hámor-Vidó, M., Jelonek, I., Johnston, M.N., Juliao-Lemus, T., Kalaitzidis, S., Knowles, W.R., Kus, J., Li, Z.S., Macleod, G., Mastalerz, M., Menezes, T.R., Ocubalidet, S., Orban, R., Pickel, W., Ranasinghe, P., Ribeiro, J., Gómez Rojas, O.P., Ruiz-Monroy, R., Schmidt, J.S., Seyedolali, A., Siavalas, G., Suarez-Ruiz, I., Vargas, C.V., Valentine, B.J., Wagner, N., Wrolson, B., Zapata, J.E.J., 2020. Testing reproducibility of vitrinite and solid bitumen reflectance measurements in North American unconventional source rock reservoir petroleum systems. Mar. Petrol. Geol. 114, 104172. https://doi.org/10.1016/j.marpetgeo.2019.104172.
Hackley, P.C., Araujo, C.V., Borrego, A.G., Bouzinos, A., Cardott, B.J., Cook, A.C., Eble, C., Flores, D., Gentzis, T., Gonçalves, P.A., Filho, J.G.M., Hámor-Vidó, M., Jelonek, I., Kommeren, K., Knowles, W., Kus, J., Mastalerz, M., Menezes, T.R., Newman, J., Oikonomopoulos, I.K., Pawlewicz, M., Pickel, W., Potter, J., Ranasinghe, P., Read, H., Reyes, J., Rodriguez, G.D.L.R., Souza, I.V.A.F., Suárez-

Ruiz, I., Sýkorová, I., Valentine, B.J., 2015. Standardization of reflectance measurements in dispersed organic matter: Results of an exercise to improve interlaboratory agreement. Mar. Petrol. Geol. 59, 22–34. https://doi.org/10.1016/j.marpetgeo.2014.07.015.

Hackley, P.C., Cardott, B.J., 2016. Application of organic petrography in North American shale petroleum systems: A review. Int. J. Coal Geol. 163, 8–51. https://doi.org/10.1016/j.coal.2016.06.010.

Hackley, P.C., Fishman, N., Wu, T., Baugher, G., 2016. Organic petrology and geochemistry of mudrocks from the lacustrine Lucaogou Formation, Santanghu Basin, northwest China: Application to lake basin evolution. Int. J. Coal Geol. 168, 20–34. https://doi.org/10.1016/j.coal.2016.05.011.

Hackley, P.C., Jubb, A.M., McAleer, R.J., Valentine, B.J., Birdwell, J.E., 2021. A review of spatially resolved techniques and applications of organic petrography in shale petroleum systems. Int. J. Coal Geol. 241, 103745. https://doi.org/10.1016/j.coal.2021.103745.

Hackley, P.C., Lewan, M., 2018. Understanding and distinguishing reflectance measurements of solid bitumen and vitrinite using hydrous pyrolysis: Implications to petroleum assessment. AAPG Bull. 102, 1119–1140. https://doi.org/10.1306/08291717097.

Hackley, P.C., Lünsdorf, N.K., 2018. Application of Raman spectroscopy as thermal maturity probe in shale petroleum systems: Insights from natural and artificial maturation series. Energy Fuel. 32 (11), 11190–11202. https://doi.org/10.1021/acs.energyfuels.8b02171.

Hackley, P.C., Sanfilipo, J.R., 2016. Organic petrology and geochemistry of Eocene Suzak bituminous marl, north-central Afghanistan: Depositional environment and source rock potential. Mar. Petrol. Geol. 73, 572–589. https://doi.org/10.1016/j.marpetgeo.2016.02.029.

Hackley, P.C., Valentine, B.J., Hatcherian, J.J., 2018. On the petrographic distinction of bituminite from solid bitumen in immature to early mature source rocks. Int. J. Coal Geol. 196, 232–245. https://doi.org/10.1016/j.marpetgeo.2016.02.029.

Hao, F., Zou, H.Y., Lu, Y.C., 2013. Mechanisms of shale gas storage: Implications for shale gas exploration in China. AAPG Bull. 97 (8), 1325–1346. https://doi.org/10.1306/02141312091.

Hao, J.Y., Zhong, N.N., Luo, Q.Y., Liu, D.H., Wu, J., Liu, A.J., 2019. Raman spectroscopy of graptolite periderm and its potential as an organic maturity indicator for the Lower Paleozoic in southwestern China. Int. J. Coal Geol. 213, 103278. https://doi.org/10.1016/j.coal.2019.103278.

Hartkopf-Fröder, C., Königshof, P., Littke, R., Schwarzbauer, J., 2015. Optical thermal maturity parameters and organic geochemical alteration at low grade diagenesis to anchimetamorphism: A review. Int. J. Coal Geol. 150–151, 74–119. https://doi.org/10.1016/j.coal.2015.06.005.

Henry, D.G., Jarvis, I., Gillmore, G., Stephenson, M., Emmings, J.F., 2018. Assessing low-maturity organic matter in shales using Raman spectroscopy: Effects of sample preparation and operating procedure. Int. J. Coal Geol. 191, 135–151. https://doi.org/10.1016/j.coal.2018.03.005.

Henry, D.G., Jarvis, I., Gillmore, G., Stephenson, M., 2019a. Raman spectroscopy as a tool to determine the thermal maturity of organic matter: Application to sedimentary, metamorphic and structural geology. Earth Sci. Rev. 198, 102936. https://doi.org/10.1016/j.earscirev.2019.102936.

Henry, D.G., Jarvis, I., Gillmore, G., Stephenson, M., 2019b. A rapid method for determining organic matter maturity using Raman spectroscopy: Application to Carboniferous organic-rich mudstones and coals. Int. J. Coal Geol. 203, 87–98. https://doi.org/10.1016/j.coal.2019.01.003.

Hou, Y.G., Zhang, K.P., Wang, F.R., He, S., Dong, T., Wang, C., Qin, W.F., Xiao, Y., Tang, B., Yu, R., Du, X.B., 2019. Structural evolution of organic matter and implications for graphitization in over-mature marine shales, south China. Mar. Petrol. Geol. 109, 304–316. https://doi.org/10.1016/j.marpetgeo.2019.06.009.

Hu, R.N., Tan, J.Q., Dick, J., Li, L., Wang, W.H., 2020. Quantification of the influences of radiolarian fossils on the pore structure of Wufeng–Lungmachi gas shales (Ordovician–Silurian) in the Sichuan Basin, South China. J. Nat. Gas Sci. Eng. 81, 103442. https://doi.org/10.1016/j.jngse.2020.103442.

Hunt, J., 1996. Petroleum Geochemistry and Geology, second ed. W.H. Freeman and Company, New York, p. 743.

Hwang, R.J., Teerman, S.C., Carlson, R.M., 1998. Geochemical comparison of reservoir solid bitumens with diverse origins. Org. Geochem. 29 (1–3), 505–517. https://doi.org/10.1016/S0146-6380(98)00078-3.

İnan, S., Goodarzi, F., Mumm, A.S., Arouri, K., Qathami, S., Ardakani, O.H., İnan, T., Tuwailib, A.A., 2016. The Silurian Qusaiba Hot Shales of Saudi Arabia: an integrated assessment of thermal maturity. Int. J. Coal Geol. 159, 107–119. https://doi.org/10.1016/j.coal.2016.04.004.

Jaboyedoff, M., Bussy, F., Kübler, B., Thelin, P., 2001. Illite "crystallinity" revisited. Clays Clay Miner. 49 (2), 156–167. https://doi.org/10.1346/CCMN.2001.0490205.

Jacob, H., 1985. Dispersed solid bitumens as an indicator for migration and maturity in prospecting for oil and gas. Erdol Kohle, ErdGas, Petrochem. 38 (8), 365.

Jacob, H., 1989. Classification, structure, genesis and practical importance of natural solid oil bitumen ("migrabitumen"). Int. J. Coal Geol. 11 (1), 65–79. https://doi.org/10.1016/0166-5162(89)90113-4.

Jarvie, D.M., Hill, R.J., Ruble, T.E., Pollastro, R.M., 2007. Unconventional shale-gas systems: Mississippian Barnett Shale of north-central Texas as one model for thermogenic shale-gas assessment. AAPG Bull. 91 (4), 475–499. https://doi.org/10.1306/12190606068.

Jubb, A.M., Botterell, P.J., Birdwell, J.E., Burruss, R.C., Hackley, P.C., Valentine, B.J., Hatcherian, J.J., Wilson, S.A., 2018. High microscale variability in Raman thermal maturity estimates from shale organic matter. Int. J. Coal Geol. 199, 1–9. https://doi.org/10.1016/j.coal.2018.09.017.

Kagi, H., Tsuchida, I., Wakatsuki, M., Takahashi, K., Kamimura, N., Iuchi, K., Wada, H., 1994. Proper understanding of down-shifted Raman spectra of natural graphite: direct estimation of laser-induced rise in sample temperature. Geochem. Cosmochim. Acta 58 (16), 3527–3530. https://doi.org/10.1016/0016-7037(94)90104-X.

Karg, H., Sauerer, B., 2022. Thermal maturity assessment of marine source rocks integrating Raman spectroscopy, organic geochemistry and petroleum systems modeling. Int. J. Coal Geol. 264 (10), 115–123. https://doi.org/10.1016/j.coal.2022.104131.

Kelemen, S.R., Fang, H.L., 2001. Maturity trends in Raman spectra from kerogen and coal. Energy Fuel. 15, 653–658. https://doi.org/10.1016/S0140-6701(02)85011-1.

Khan, I., Zhong, N.N., Luo, Q.Y., Ai, J.Y., Yao, L.P., Luo, P., 2020. Maceral composition and origin of organic matter input in Neoproterozoic–Lower Cambrian organic-rich shales of Salt Range Formation, upper Indus Basin, Pakistan. Int. J. Coal Geol. 217, 103319. https://doi.org/10.1016/j.coal.2019.103319.

Khatibi, S., Ostadhassan, M., Hackley, P., Tuschel, D., Abarghani, A., Bubach, B., 2019. Understanding organic matter heterogeneity and maturation rate by Raman spectroscopy. Int. J. Coal Geol. 206, 46–64. https://doi.org/10.1016/j.coal.2019.03.009.

Khavari-Khorasani, G., 1983. Structure of albertite from New Brunswick, Canada. Bull. Can. Petrol. Geol. 31 (2), 123–126. https://doi.org/10.35767/gscpgbull.31.2.123.

Khorasani, G.K., Michelsen, J.K., 1993. The thermal evolution of solid bitumens, bitumen reflectance, and kinetic modeling of reflectance: Application in petroleum and ore prospecting. Energy Sourc. 15, 181–204. https://doi.org/10.1080/00908319308909024.

Kibria, M.G., Das, S., Hu, Q.H., et al., 2020. Thermal maturity evaluation using Raman spectroscopy for oil shale samples of USA: Comparisons with vitrinite reflectance and pyrolysis methods. Pet. Sci. 17 (3), 567–581. https://doi.org/10.1007/s12182-020-00443-z.

Kouketsu, Y., Mizukami, T., Mori, H., Endo, S., Aoya, M., Hara, H., Nakamura, D., Wallis, S., 2014. A new approach to develop the Raman carbonaceous material geothermometer for low-grade metamorphism using peak width. Isl. Arc 23, 33–50. https://doi.org/10.1111/iar.12057.

Kübler, B., Jaboyedoff, M., 2000. Illite crystallinity. C. R. Acad. Sci. II 331 (2), 75–89. https://doi.org/10.1016/S1251-8050(00)01395-1.

Kus, J., Araujo, C.V., Borrego, A.G., Flores, D., Hackley, P.C., Hámor-Vidó, M., Kalaitzidis, S., Kommeren, C.J., Kwiecińska, B., Mastalerz, M., Mendonça Filho, J.G., Menezes, T.R., Misz-Kennan, M., Nowak, G.J., Petersen, H.I., Rallakis, D., I. Suárez-Ruiz, I., Sýkorová, I., Životić, D., 2017. Identification of alginite and bituminite in rocks other than coal. 2006, 2009, and 2011 round robin exercises of the ICCP identification of Dispersed Organic Matter Working Group. Int. J. Coal Geol. 178, 26–38. https://doi.org/10.1016/j.coal.2017.04.013.

Landis, C.R., Castaño, J.R., 1995. Maturation and bulk chemical properties of a suite of solid hydrocarbons. Org. Geochem. 22 (1), 137–149. https://doi.org/10.1016/0146-6380(95)90013-6.

Lavoie, D., Pinet, N., Bordeleau, G., Ardakani, O.H., Ladevèze, P., Duchesne, M.J., Rivard, C., Mort, A., Brake, V., Sanei, H., Malet, X., 2016. The Upper Ordovician black shales of southern Quebec (Canada) and their significance for naturally occurring hydrocarbons in shallow groundwater. Int. J. Coal Geol. 158, 44–64. https://doi.org/10.1016/j.coal.2016.02.008.

Lespade, P., Al-Jishi, R., Dresselhaus, M.S., 1982. Model for Raman scattering from incompletely graphitized carbons. Carbon 20, 427–431. https://doi.org/10.1016/0008-6223(82)90043-4.

Li, X.Z., Hayashi, J.-I., Li, C.Z., 2006. FT-Raman spectroscopic study of the evolution of char structure during the pyrolysis of a Victorian brown coal. Fuel 85, 1700–1707. https://doi.org/10.1016/j.fuel.2006.03.008.

Li, C.Z., Dou, P., Dou, S., Wen, G.H., 2024. Progress in the study of solid asphalt morphology, genesis, and applications. Acta Sedimentol. Sin. 42 (5), 1479–1493. https://doi.org/10.14027/j.issn.1000-0550.2023.048 (in Chinese).

Link, C., Bustin, R., Goodarzi, F., 1990. Petrology of graptolites and their utility as indices of thermal maturity in Lower Paleozoic strata in northern Yukon, Canada. Int. J. Coal Geol. 15, 113–135. https://doi.org/10.1016/0166-5162(90)90007-L.

Liu, B., Mastalerz, M., Schieber, J., 2022. SEM petrography of dispersed organic matter in black shales: A review. Earth Sci. Rev. 224, 103874. https://doi.org/10.1016/j.earscirev.2021.103874.

Liu, B., Schieber, J., Mastalerz, M., 2019. Petrographic and micro-FTIR study of organic matter in the Devonian New Albany Shale during thermal maturation: Implications for kerogen transformation. Mudstone diagenersis: Research perspectives for shale hydrocarbon reservoirs, seals and source rocks. AAPG Memoir 120, Tulsa, pp. 165–188. https://doi.org/10.1306/13672216M1213380.

Liu, B., Wang, L., Fu, X.F., Huo, Q.L., Bai, L.H., Lyu, J.C., Wang, B.Y., 2023. Identification, evolution and geological indications of solid bitumen in shales: A case study of the first member of Cretaceous Qingshankou Formation in Songliao Basin, NE China. Petrol. Explor. Dev. 50, 1345–1357. https://doi.org/10.1016/S1876-3804(24)60471-4.

Liu, D.H., Shi, J.Y., 1994. Discussion on unconventional evaluation method of high maturity carbonate source rocks. Petrol. Explor. Dev. 21 (3), 113–115.

Liu, D.H., Xiao, X.M., Tian, H., Min, Y.S., Zhou, Q., Cheng, P., Shen, J.G., 2013. Sample maturation calculated using Raman spectroscopic parameters for solid organics: Methodology and geological applications. Chin. Sci. Bull. 58, 1285–1298. https://doi.org/10.1007/s11434-012-5535-y.

Liu, D.M., Hou, X.Q., Jiang, J.P., 1996. The composition and structure of graptolite-a micro-area analysis. Acta Mineral. Sin. 16, 53–57 (in Chinese).

Liu, Q., Mambwe, P., Littke, R., Muchez, P., 2024. Diagenesis and mineralization in the Central African Copperbelt, implications from the reflectance of pyrobitumen and Kübler (illite crystallinity) index. Int. J. Coal Geol. 289, 104534. https://doi.org/10.1016/j.coal.2024.104534.

Liu, S.Y., Gao, P., Xiao, X.M., Liu, R.B., Qin, J., Yuan, T., Wang, X., 2022. Study on organic petrology characteristics of the Wufeng-Longmaxi formations black shale, Sichuan Basin. Geoscience 36, 1281. https://doi.org/10.19657/j.geoscience.1000-8527.2022.046 (in Chinese).

Liu, W., Gao, P., Xiao, X.M., Zhao, Y.M., Xing, Y.J., Li, J.K., 2024. Variable depositional environments and organic matter enrichment of early Cambrian shales in the Middle Yangtze region, South China. J. Asian Earth Sci. 259, 105874. https://doi.org/10.1016/j.jseaes.2023.105874.

Loucks, R.G., Reed, R.M., Ruppel, S.C., Jarvie, D.M., 2009. Morphology, genesis, and distribution of nanometer-scale pores in siliceous mudstones of the Mississippian Barnett Shale. J. Sediment. Res. 79 (12), 848–861. https://doi.org/10.2110/jsr.2009.092.

Loucks, R.G., Reed, R.M., Ruppel, S.C., Hammes, U., 2012. Spectrum of pore types and networks in mudrocks and a descriptive classifcation for matrix-related mudrock pores. AAPG Bull. 96, 1071–1098. https://doi.org/10.1306/08171111061.

Lu, L.F., Qin, J.Z., Shen, B.J., Borjigin, T., Liu, W.X., Zhang, Q.Z., 2016. Biogenic origin and hydrocarbon significance of siliceous shale from the Wufeng–Longmaxi formations in Fuling area, southeastern Sichuan Basin. Exp. Pet. Geol. 38, 460–465. https://doi.org/10.11781/sysydz201604460 (in Chinese).

Luo, Q.Y., Fariborz, G., Zhong, N.N., Wang, Y., Qiu, N.S., Skovsted, C.B., Suchý, V., Schovsbo, N.H., Morga, R., Xu, Y.H., Hao, J.Y., Liu, A.J., Wu, J., Cao, W.X., Min, X., Wu, J., 2020. Graptolites as fossil geo-thermometers and source material of hydrocarbons: An overview of four decades of progress. Earth Sci. Rev. 200, 103000. https://doi.org/10.1016/j.earscirev.2019.103000.

Luo, Q.Y., Hao, J.Y., Skovsted, C.B., Luo, P., Khan, I., Wu, J., Zhong, N.N., 2017. The organic petrology of graptolites and maturity assessment of the Wufeng–Longmaxi formations from Chongqing, China: Insights from reflectance cross-plot analysis. Int. J. Coal Geol. 183, 161–173. https://doi.org/10.1016/j.coal.2017.09.006.

Luo, Q.Y., Hao, J.Y., Skovsted, C.B., Xu, Y.H., Liu, Y., Wu, J., Zhang, S.N., Wang, W.L., 2018. Optical characteristics of graptolite-bearing sediments and its implication for thermal maturity assessment. Int. J. Coal Geol. 195, 386–401. https://doi.org/10.1016/j.coal.2018.06.019.

Luo, Q.Y., Zhang, L., Zhong, N.N., Wu, J., Goodarzi, F., Sanei, H., Skovsted, C.B., Suchý, V., Li, M.J., Ye, X.Z., Cao, W.X., Liu, A.J., Min, X., Pan, Y.Y., Yao, L.P., Wu, J., 2021. Thermal evolution behavior of the organic matter and a ray of light on the origin of vitrinite-like maceral in the Mesoproterozoic and Lower Cambrian black shales: Insights from artificial maturation. Int. J. Coal Geol. 244. https://doi.org/10.1016/j.coal.2021.103813.

Luo, Q., Zhong, N., Dai, N., Zhang, W., 2016. Graptolite-derived organic matter in the Wufeng–Longmaxi formations (Upper Ordovician–Lower Silurian) of southeastern Chongqing, China: Implications for gas shale evaluation. Int. J. Coal Geol. 153, 87–98. https://doi.org/10.1016/j.coal.2015.11.014.

Luo, Q.Y., Zhong, N.N., Li, M.J., Wu, J., Khan, I., Zhang, Y., Chen, Q., Ye, X.Z., Li, W.H., Ji, W.M., Liu, A.J., Hao, J.Y., Yao, L.P., Wu, L., 2023. Classification, origins, and evolution of macerals in the Precambrian–Eopaleozoic sedimentary rocks. Oil Gas Geol. 44 (5), 1084–1101. https://doi.org/10.11743/ogg20230502 (in Chinese).

Luo, Q.Y., Zhong, N.N., Qin, J., Li, K.W., Zhang, Y.Q., Wang, Y.N., Ma, L., 2014. Thucholite in Mesoproterozoic shales from northern North China: Occurrence and indication for thermal maturity. Int. J. Coal Geol. 125, 1–9. https://doi.org/10.1016/j.coal.2014.01.009.

Lupoi, J.S., Hackley, P.C., Birsic, E., Fritz, L.P., Solotky, L., Weislogel, A., Schlaegle, S., 2019. Quantitative evaluation of vitrinite reflectance in shale using Raman spectroscopy and multivariate analysis. Fuel 254, 115573. https://doi.org/10.1016/j.fuel.2019.05.156.

Lünsdorf, N.K., 2016. Raman spectroscopy of dispersed vitrinite-methodical aspects and correlation with reflectance. Int. J. Coal Geol. 153, 75–86. https://doi.org/10.1016/j.coal.2015.11.010.

Machel, H.G., 2001. Bacterial and thermochemical sulfate reduction in diagenetic settings—old and new insights. Sediment. Geol. 140, 143–175. https://doi.org/10.1016/S0037-0738(00)00176-7.

Mählmann, R.F., Le Bayon, R., 2016. Vitrinite and vitrinite like solid bitumen reflectance in thermal maturity studies: Correlations from diagenesis to incipient metamorphism in different geodynamic settings. Int. J. Coal Geol. 157, 52–73. https://doi.org/10.1016/j.coal.2015.12.008.

Marques, M., Suárez-Ruiz, I., Flores, D., Guedes, A., Rodrigues, S., 2009. Correlation between optical, chemical and micro-structural parameters of high-rank coals and graphite. Int. J. Coal Geol. 77, 377–382. https://doi.org/10.1016/j.coal.2008.06.002.

Mastalerz, M., Bustin, R.M., Sinclair, A.J., Stankiewicz, B.A., 1995. Carbon-rich material in the Erickson hydrothermal system, northern British Columbia, Canada; origin and formation mechanisms. Econ. Geol. 90, 938–947. https://doi.org/10.2113/gsecongeo.90.4.938.

Mastalerz, M., Drobniak, A., Stankiewicz, A.B., 2018. Origin, properties, and implications of solid bitumen in source-rock reservoirs: A review. Int. J. Coal Geol. 195, 14–36. https://doi.org/10.1016/j.coal.2018.05.013.

Mastalerz, M., Schimmelmann, A., Drobniak, A., Chen, Y.Y., 2013. Porosity of Devonian and Mississippian New Albany Shale across a maturation gradient: Insights from organic petrology, gas adsorption, and mercury intrusion. AAPG Bull. 97, 1621–1643. https://doi.org/10.1306/04011312194.

Mathew, G., De Sarkar, S., Pande, K., Dutta, S., Ali, S., Rai, A., Netrawali, S., 2013. Thermal metamorphism of the Arunachal Himalaya, India: Raman thermometry and thermochronological constraints on the tectono-thermal evolution. Int. J. Earth Sci. 102 (7), 1911–1936. https://doi.org/10.1007/s00531-013-0904-6.

Meng, G.M., Gai, H.F., Yang, X.M., Gao, P., Zhou, Q., Lu, C.G., Li, G., Wang, X., Cheng, P., 2024. Occurrence and maturation transformation of organic and inorganic nitrogen in the Lower Cambrian shelf–slope facies shale: Implications for overmature N_2-rich shale reservoirs in Southern China. Mar. Petrol. Geol. 168, 107011. https://doi.org/10.1016/j.marpetgeo.2024.107011.

Meng, J.H., Lyu, P.X., Wu, W., Pan, R.F., Zhu, Y.Q., 2022. A method for evaluating the thermal maturity of marine shale based on graptolite reflectance and Raman spectroscopy: a case from the Lower Palaeozoic Wufeng–Longmaxi Formations, southern Sichuan Basin, SW China. Oil Gas Geol. 43, 1515–1528. https://doi.org/10.11743/ogg20220620 (in Chinese).

Misch, D., Gross, D., Hawranek, G., Horsfield, B., Klaver, J., Mendez-Martin, F., Urai, J.L., Vranjes-Wessely, S., Sachsenhofer, R.F., Schmatz, J., Li, J., Zou, C., 2019. Solid bitumen in shales: Petrographic characteristics and implications for reservoir characterization. Int. J. Coal Geol. 205, 14–31. https://doi.org/10.1016/j.coal.2019.02.012.

Montgomery, S.L., Jarvie, D.M., Bowker, K.A., Pollastro, R.M., 2005. Mississippian Barnett shale, Fort Worth Basin, north-central Texas: Gas-shale play with multi-trillion cubic foot potential. AAPG Bull. 89 (2), 155–175. https://doi.org/10.1306/09170404042.

Moore, R.C., 1955. Treatise on Invertebrate Paleontology, Part V, Graptolithina. Kansas, Geol. Soc. Am. University of Kansas Press.

Mukherjee, M.K., Modak, K., Ghosh, J., 2019. Illite crystallinity index from the Mesoproterozoic sedimentary cover of the Kaladgi basin, southwestern India: Implications on crustal depths of subsidence and deformation. J. Earth Syst. Sci. 128, 1–15. https://doi.org/10.1007/s12040-019-1124-7.

Mukhopadhyay, P.K., Hagemann, H.W., Gormly, J.R., 1985. Characterization of kerogens as seen under the aspects of maturation and hydrocarbon generation. Erdol Kohle, ErdGas, Petrochem. 38, 7–18.

Newman, J., Edman, J., Howe, J., LeFever, J.. The Bakken at Parshall Field: Inferences from New Data Regarding Hydrocarbon Generation and Migration. https://doi.org/10.1190/urtec2013-037.

Obermajer, M., Fowler, M.G., Goodarzi, F., Snowdon, L.R., 1996. Assessing thermal maturity of Palaeozoic rocks from reflectance of chitinozoa as constrained by geochemical indicators: An example from southern Ontario, Canada. Mar. Petrol. Geol. 13 (8), 907–919. https://doi.org/10.1016/S0264-8172(96)00036-0.

Obermajer, M., Fowler, M.G., Snowdon, L.R., 1999. Depositional environment and oil generation in Ordovician source rocks from Southwestern Ontario, Canada: Organic geochemical and petrological Approach1. AAPG Bull. 83 (9), 1426–1453. https://doi.org/10.1306/E4FD41D9-1732-11D7-8645000102C1865D.

Pasteris, J.D., Wopenka, B., 1991. Raman spectra of graphite as indicators of degree of metamorphism. Can. Mineral. 29, 1–9.

Petersen, H.I., Schovsbo, N.H., Nielsen, A.T., 2013. Reflectance measurements of zooclasts and solid bitumen in Lower Paleozoic shales, southern Scandinavia: Correlation to vitrinite reflectance. Int. J. Coal Geol. 114, 1–18. https://doi.org/10.1016/j.coal.2013.03.013.

Pickel, W., Kus, J., Flores, D., Kalaitzidis, S., Christanis, K., Cardott, B.J., Misz-Kennan, M., Rodrigues, S., Hentschel, A., Hamor-Vido, M., Crosdale, P., Wagner, N., ICCP, 2017. Classification of liptinite–ICCP System 1994. Int. J. Coal Geol. 169, 40–61. https://doi.org/10.1016/j.coal.2016.11.004.

Pimenta, M.A., Dresselhaus, G., Dresselhaus, M.S., Cançado, L.G., Jorio, A., Saito, R., 2007. Studying disorder in graphite-based systems by Raman spectroscopy. Phys. Chem. Chem. Phys. 9 (11), 1276–1290. https://doi.org/10.1039/B613962K.

Rahmani, A., Naderi, M., Hosseiny, E., 2022. Shale gas potential of the lower Silurian hot shales in southern Iran and the Arabian Plate: Characterization of organic geochemistry. Petroleum 9 (4), 499–507. https://doi.org/10.1016/j.petlm.2022.03.004.

Rantitsch, G., Grogger, W., Teichert, C., Ebner, F., Hofer, C., Maurer, E.M., Schaffer, B., Toth, M., 2004. Conversion of carbonaceous material to graphite within the Greywacke Zone of the Eastern Alps. Int. J. Earth Sci. 93 (6), 959–973. https://doi.org/10.1007/s00531-004-0436-1.

Rantitsch, G., Lammerer, W., Fisslthaler, E., Mitsche, S., Kaltenböck, H., 2016. On the discrimination of semi-graphite and graphite by Raman spectroscopy. Int. J. Coal Geol. 159, 49–56. https://doi.org/10.1016/j.coal.2016.04.001.

Reich, S., Thomsen, C., 2004. Raman spectroscopy of graphite. Philos. Trans. R. Soc. A Math. Phys. Eng. Sci. 362 (1824), 2271–2288. https://doi.org/10.1098/rsta.2004.1454.

Reyes, J., Jiang, C., Lavoie, D., Armstrong, D.K., Milovic, M., Robinson, R., 2018. Organic petrographic analysis of artificially matured chitinozoan- and graptolite-rich Upper Ordovician shale from Hudson Bay Basin, Canada. Int. J. Coal Geol. 199, 138–151. https://doi.org/10.1016/j.coal.2018.09.019.

Riediger, C., 1993. Solid bitumen reflectance and Rock-Eval T_{max} as maturation indices: An example from the "Nordegg Member", Western Canada Sedimentary Basin. Int. J. Coal Geol. 22, 295–315. https://doi.org/10.1016/0166-5162(93)90031-5.

Rippen, D., Littke, R., Bruns, B., Mahlstedt, N., 2013. Organic geochemistry and petrography of Lower Cretaceous Wealden black shales of the Lower Saxony Basin: the transition from lacustrine oil shales to gas shales. Org. Geochem. 63, 18–36. https://doi.org/10.1016/j.orggeochem.2013.07.013.

Ruppert, L.F., Sakurovs, R., Blach, T.P., He, L., Melnichenko, Y.B., Mildner, D.F.R., Alcantar-Lopez, L., 2013. A USANS/SANS study of the accessibility of pores in the Barnett shale to methane and water. Energy Fuel. 27, 772–779. https://doi.org/10.1021/ef301859s.

Sanei, H., 2020. Genesis of solid bitumen. Sci. Rep. 10 (1), 15595. https://doi.org/10.1038/s41598-020-72692-2.

Sanei, H., Ardakani, O.H., 2016. Alteration of organic matter by ion milling. Int. J. Coal Geol. 163, 123–131. https://doi.org/10.1016/j.coal.2016.06.021.

Sanei, H., Haeri-Ardakani, O., Wood, J.M., Curtis, M.E., 2015. Effects of nanoporosity and surface imperfections on solid bitumen reflectance (BR_o) measurements in unconventional reservoirs. Int. J. Coal Geol. 138, 95–102. https://doi.org/10.1016/j.coal.2014.12.011.

Sanei, H., Petersen, H.I., Schovsbo, N.H., Jiang, C., Goodsite, M.E., 2014. Petrographic and geochemical composition of kerogen in the Furongian (U. Cambrian) Alum Shale, central Sweden: reflections on the petroleum generation potential. Int. J. Coal Geol. 132, 158–169. https://doi.org/10.1016/j.coal.2014.08.010.

Sauerer, B., Craddock, P.R., AlJohani, M.D., Alsamadony, K.L., Abdallah, W., 2017. Fast and accurate shale maturity determination by Raman spectroscopy measurement with minimal sample preparation. Int. J. Coal Geol. 173, 150–157. https://doi.org/10.1016/j.coal.2017.02.008.

Schmidt, J.S., Araujo, C.V., Souza, I.V.A.F., Chagas, R.B.A., 2015. Hydrous pyrolysis maturation of vitrinite-like and humic vitrinite macerals: Implications for thermal maturity analysis. Int. J. Coal Geol. 144–145, 5–14. https://doi.org/10.1016/j.coal.2015.03.016.

Schmidt, J.S., Menezes, T.R., Souza, I.V.A.F., Spigolon, A.L.D., Pestilho, A.L.S., Coutinho, L.F.C., 2019. Comments on empirical conversion of solid bitumen reflectance for thermal maturity evaluation. Int. J. Coal Geol. 201, 44–50. https://doi.org/10.1016/j.coal.2018.11.012.

Schmidt, M.A., İnan, S., 2016. Microscale organic maturity determination of graptolites using Raman spectroscopy. Int. J. Coal Geol. 162, 96-107. https://doi.org/10.1016/j.coal.2016.05.002.

Schito, A., Corrado, S., Aldegal, L., Grigo, D., 2016. Overcoming pitfalls of vitrinite reflectance measurements in the assessment of thermal maturity: the case history of the lower Congo Basin. Mar. Petrol. Geol. 74, 59–70. https://doi.org/10.1016/j.marpetgeo.2016.04.002.

Schito, A., Muirhead, D., Parnell, J., 2023. Towards a kerogen-to-graphite kinetic model by means of Raman spectroscopy. Earth Sci. Rev. 237, 104292. https://doi.org/10.1016/j.earscirev.2022.104292.

Schito, A., Romano, C., Corrado, S., Grigo, D., Poe, B., 2017. Diagenetic thermal evolution of organic matter by Raman spectroscopy. Org. Geochem. 106, 57–67. https://doi.org/10.1016/j.orggeochem.2016.12.006.

Schoenherr, J., Littke, R., Urai, J.L., Kukla, P.A., Rawahi, Z., 2007. Polyphase thermal evolution in the Infra-Cambrian are Group (South Oman Salt Basin) as deduced by maturity of solid reservoir bitumen. Org. Geochem. 38 (8), 1293–1318. https://doi.org/10.1016/j.orggeochem.2007.03.010.

Song, J.Y., Hackley, P.C., Sanders, M.M., Jubb, A.M., Luo, Q.Y., 2023. Thermal evolution of graptolite and solid bitumen properties at high maturity under natural and artificial conditions. Int. J. Coal Geol. 273, 104269. https://doi.org/10.1016/j.coal.2023.104269.

Spötl, C., Houseknecht, D.W., Jaques, R.C., 1998. Kerogen maturation and incipient graphitization of hydrocarbon source rocks in the Arkoma Basin, Oklahoma and Arkansas: A combined petrographic and Raman spectrometric study. Org. Geochem. 28, 535–542. https://doi.org/10.1016/S0146-6380(98)00021-7.

Stasiuk, L.D., 1997. The origin of pyrobitumens in Upper Devonian Leduc Formation gas reservoirs, Alberta, Canada: An optical and EDS study of oil to gas transformation. Mar. Petrol. Geol. 14, 915–929. https://doi.org/10.1016/S0264-8172(97)00031-7.

Stefanopoulos, K.L., Youngs, T.G., Sakurovs, R., Ruppert, L.F., Bahadur, J., Melnichenko, Y.B., 2017. Neutron scattering measurements of carbon dioxide adsorption in pores within the marcellus shale: Implications for sequestration. Environ. Sci. Technol. 51, 6515–6521. https://doi.org/10.1021/acs.est.6b05707.

Stokes, M.R., Jubb, A.M., Hackley, P.C., Birdwell, J.E., Barnhart, E.P., Scott, C.T., Shelton, J.L., Sanders, M.M., Hatcherian, J.J., 2023. Evaluation of portable Raman spectroscopic analysis for source-rock thermal maturity assessments on bulk crushed rock. Int. J. Coal Geol. 279, 104374. https://doi.org/10.1016/j.coal.2023.104374.

Suárez-Ruiz, I., Flores, D., Mendonça Filho, J.G., Hackley, P.C., 2012. Review and update of the applications of organic petrology: Part 1, geological applications. Int. J. Coal Geol. 99, 54–112. https://doi.org/10.1016/j.coal.2012.02.004.

Synnott, D.P., Dewing, K., Ardakani, O.H., Obermajer, M., 2018. Correlation of zooclast reflectance with Rock-Eval Tmax values within Upper Ordovician Cape Phillips Formation, a potential petroleum source rock from the Canadian Arctic Islands. Fuel 227, 165–176. https://doi.org/10.1016/j.fuel.2018.04.096.

Tan, J.Q., Hu, R.N., Wang, W.H., Dick, J., 2020. Palynological analysis of the Late Ordovician–early Silurian black shales in South China provides new insights for the investigation of pore systems in shale gas reservoirs. Mar. Petrol. Geol. 116, 104145. https://doi.org/10.1016/j.marpetgeo.2019.104145.

Taylor, G.H., Liu, S.Y., 1989. Micrinite—its origin and significance. Int. J. Coal Geol. 14, 29–46. https://doi.org/10.1016/0166-5162(89)90077-3.

Taylor, G.H., Teichmüller, M., Davis, A., Diessel, C.F.K., Littke, R., Robert, P., 1998. Organic Petrology. Gebruder Borntraeger, Berlin and Stuttgart, p. 704.

Teichmüller, M., 1986. Organic petrology of source rocks, history and state of the art. Org. Geochem. 10 (1), 581–599. https://doi.org/10.1016/0146-6380(86)90055-0.

Tewalt, S.J., Belkin, H.E., SanFilipo, J.R., Merrill, M.D., Palmer, C.A., Warwick, P.D., Karlsen, A.W., Finkelman, R.B., Park, A.J., 2010. Chemical analyses in the World Coal Quality Inventory, version 1: U.S. Geological Survey Open-File Report 2010–1196.

Tissot, B., Welte, D.H., 1984. Petroleum Formation and Occurrence, second ed. Springer, Berlin, p. 699.

Tricker, P.M., Marshall, J.E.A., Badman, T.D., 1992. Chitinozoan reflectance: a Lower Palaeozoic thermal maturity indicator. Mar. Petrol. Geol. 9 (3), 302–307. https://doi.org/10.1016/0264-8172(92)90078-S.

Tuinstra, F., Koenig, J.L., 1970. Raman spectrum of graphite. J. Chem. Phys. 53, 1126–1130.

Valentine, B.J., Hackley, P.C., Enomoto, C.B., Bove, A.M., Dulong, F.T., Lohr, C.D., Scott, K.R., 2014. Organic petrology of the Aptian-age section in the downdip Mississippi Interior Salt Basin, Mississippi, USA: Observations and preliminary implications for thermal maturation history. Int. J. Coal Geol. 131, 378–391. https://doi.org/10.1016/j.coal.2014.07.001.

Van Gijzel, P., 1981. Applications of geomicrophotometry of kerogen, solid hydrocarbons and crude oils to petroleum exploration. In: Brooks, J. (Ed.), Organic Maturation Studies and Fossil Fuel Exploration. Academic Press, New York, pp. 351–377.

Varol, N., Demirel, İ.H., 2020. Hydrocarbon potential of the Silurian and Carboniferous shales in the Western and Central Taurus Region of Turkey. Int. J. Coal Geol. 227, 103518. https://doi.org/10.1016/j.coal.2020.103518.

Vidano, R.P., Fischbach, D.B., Willis, L.J., Loehr, T.M., 1981. Observation of Raman band shifting with excitation wavelength for carbons and graphites. Solid State Commun. 39 (2), 341–344. https://doi.org/10.1016/0038-1098(81)90686-4.

Waliczek, M., Machowski, G., Więcław, D., Konon, A., Wandycz, P., 2019. Properties of solid bitumen and other organic matter from Oligocene shales of the Fore-Magura Unit in Polish Outer Carpathians: Microscopic and geochemical approach. Int. J. Coal Geol. 210, 103206. https://doi.org/10.1016/j.coal.2019.05.013.

Wang, F.Y., Chen, J.Y., Gao, G., Sun, Y.G., Peng, P.A., 2010. Reflectance of macroalgae-derived vitrinite-like macerals: An organic maturity indicator for Pre-Devonian marine strata. Petrol. Explor. Dev. 37 (2), 250–256, 1000-0747(2010)02-0250-07.

Wang, F.Y., He, P., Cheng, D.S., Hao, S.S., Liu, D.H., 1996. Take Vitrinite-like reflectance as the maturity indicator for Lower Paleozoic high-over mature source rock. Nat. Gas. Ind. 16 (4), 24–28 (in Chinese).

Wang, Q., Qian, M.H., Jiang, Q.G., Yang, Y.F., Borjigin, T., 2017. A study on hydrocarbon generation capacity of graptolite in marine hydrocarbon source rocks in southern China. Rock Miner. Anal. 36, 258–264. https://doi.org/10.15898/j.cnki.11-2131/td.201611170173 (in Chinese).

Wang, Y., Hu, K., 2002. Using laser Raman spectrum parameters as indicators of maturation for organic carbon. J. Mineral. Petrol. 22, 57–60. https://doi.org/10.19719/j.cnki.1001-6872.2002.03.01 (in Chinese).

Wang, Y., Qiu, N.S., Borjigin, T., Shen, B.J., Xie, X.M., Ma, Z.L., Lu, C.J., Yang, Y.F., Yang, L., Cheng, L.J., Fang, G.J., Cui, Y., 2019. Integrated assessment of thermal maturity of the Upper Ordovician–Lower Silurian Wufeng–Longmaxi shale in Sichuan Basin, China. Mar. Petrol. Geol. 100, 447–465. https://doi.org/10.1016/j.marpetgeo.2018.10.025.

Wang, Y., Qiu, N.S., Ma, Z.L., Ning, C.X., Zheng, L.J., Zhou, Y.Y., Fang, G.J., Rui, X.Q., Rao, D., 2020. Evaluation of equivalent relationship between vitrinite reflectance and solid bitumen reflectance. J. China Univ. Min. Tech. 49, 563–575. https://doi.org/10.13247/j.cnki.jcumt.001114 (in Chinese).

Wang, Y., Qiu, N., Xie, X., Ma, Z., Li, L., Feng, Q., Yang, L., Shen, B., Borjigin, T., Tao, N., 2021. Maturity and thermal evolution differences between two sets of Lower Palaeozoic shales and its significance for shale gas formation in south-western Sichuan Basin, China. Geol. J. 56 (7), 3698–3719. https://doi.org/10.1002/gj.4121.

Wang, Y.F., Xie, L.F., Li, J., Han, S.B., Qiao, Y., Wang, J., Yang, C.L., Xie, Z.Y., 2023. Characteristics evaluation of high-over mature organic matter based on laser Raman and Fourier transform mass spectrometry experiments. Nat. Gas. Ind. 43 (11), 83–99. https://doi.org/10.3787/j.issn.1000-0976.2023.11.008.

Wei, L., Mastalerz, M., Schimmelmann, A., Chen, Y., 2014. Influence of Soxhlet-extractable bitumen and oil on porosity in thermally maturing organic-rich shales. Int. J. Coal Geol. 132, 38–50. https://doi.org/10.1016/j.coal.2014.08.003.

Wei, L., Wang, Y., Mastalerz, M., 2016. Comparative optical properties of macerals and statistical evaluation of mis-identification of vitrinite and solid bitumen from early mature Middle Devonian – Lower Mississippian New Albany Shale: implications for thermal maturity assessment. Int. J. Coal Geol. 168, 222–236. https://doi.org/10.1016/j.coal.2016.11.003.

Wilkins, R.W.T., Boudou, R., Sherwood, N., Xiao, X.M., 2014. Thermal maturity evaluation from inertinites by Raman spectroscopy: The 'RaMM' technique. Int. J. Coal Geol. 128–129, 143–152. https://doi.org/10.1016/j.coal.2014.03.006.

Wilkins, R.W.T., Wang, M., Gan, H., Li, Z.S., 2015. A RaMM study of thermal maturity of dispersed organic matter in marine source rocks. Int. J. Coal Geol. 150–151, 252–264. https://doi.org/10.1016/j.coal.2015.09.007.

Wilson, N.S., 2000. Organic petrology, chemical composition, and reflectance of pyrobitumen from the El Soldado Cu deposit, Chile. Int. J. Coal Geol. 43, 53–82. https://doi.org/10.1016/S0166-5162(99)00054-3.

Wopenka, B., Pasteris, J.D., 1993. Structural characterization of kerogens to granulitefacies graphite: applicability of Raman microprobe spectroscopy. Am. Mineral. 78, 533–577.

Wu, J., Luo, Q.Y., Zhang, Y., Zhong, N.N., Goodarzi, F., Suchý, V., Li, M.J., Li, D.H., Wang, W.X., Tian, X.W., Song, Z.Z., 2023. The organic petrology of vitrinite-like maceral in the Lower Paleozoic shales: Implications for the thermal maturity evaluation. Int. J. Coal Geol. 274. https://doi.org/10.1016/j.coal.2023.104282.

Xiao, X.M., Liu, D.H., Fu, J.M., 1991. The significance of bitumen reflectance as a mature parameter of source rocks. Acta Sedimentol. Sin. (S1), 138–146. https://doi.org/10.14027/j.cnki.cjxb.1991.s1.019.

Xiao, X.M., Wang, M.L., Wei, Q., Tian, H., Pan, Y., Li, T.F., 2015. Evaluation of Lower Paleozoic shale with shale gas prospect in south China. Nat. Gas Geosci. 26, 1433–1445. https://doi.org/10.11764/j.issn.1672-1926.2015.08.1433.

Xiao, X.M., Wilkins, R., Liu, D., Liu, Z.F., Fu, J.M., 2000. Investigation of thermal maturity of lower Palaeozoic hydrocarbon source rocks by means of vitrinite-like maceral reflectance–a Tarim Basin case study. Org. Geochem. 31, 1041–1052. https://doi.org/10.1016/S0146-6380(00)00061-9.

Xiao, X.M., Zhou, Q., Cheng, P., Sun, J., Liu, D.H., Tian, H., 2020. Thermal maturation as revealed by micro-raman spectroscopy of mineral-organic aggregation (MOA) in marine shales with high and over maturities. Sci. China Earth Sci. 63, 1540–1552. https://doi.org/10.1007/s11430-020-9627-2.

Xing, Y.J., Xiao, X.M., Zhou, Q., Liu, W., Zhao, Y.M., 2023. Influence of water on the methane adsorption capacity of organic-rich shales and its controlling factors: A review. Energies 16 (8). https://doi.org/10.3390/en16083305.

Xu, L., Yang, W., Jiang, Z., Chen, D.X., Wang, Y.H., Lu, J.K., Zhao, M.Z., Li, L., 2022. Evolution and genesis of organic pores in Triassic Xujiahe Formation shale, Western Sichuan Depression, Sichuan Basin. Oil Gas Geol. 43 (2), 325–340. https://doi.org/10.11743/ogg20220207.

Yang, S., Horsfield, B., 2020. Critical review of the uncertainty of Tmax in revealing the thermal maturity of organic matter in sedimentary rocks. Int. J. Coal Geol. 225, 103500. https://doi.org/10.1016/j.coal.2020.103500.

Yang, X., Liu, C., Liu, W., et al., 2021. Characteristics of and factors influencing organic pores in the Lower Silurian Longmaxi Formation, Fushun-Yongchuan area, Sichuan Basin. Oil Gas Geol. 42 (6), 1321–1333. https://doi.org/10.11743/ogg20210607.

Yui, T.F., Huang, E., Xu, J., 1996. Raman spectrum of carbonaceous material: a possible metamorphic grade indicator for low-grade metamorphic rocks. J. Metamorph. Geol. 14, 115–124. https://doi.org/10.1046/j.1525-1314.1996.05792.x.

Zhang, Y., Li, Z., 2019. Raman spectroscopic study of chemical structure and thermal maturity of vitrinite from a suite of Australia coals. Fuel 241, 188–198. https://doi.org/10.1016/j.fuel.2018.12.037.

Zhao, Y.M., Gao, P., Zhou, Q., Xiao, X.M., Xing, Y.J., Liu, W., 2022. A review of the heterogeneity of organic-matter-hosted pores in shale reservoirs. Energies 15 (23). https://doi.org/10.3390/en15238805.

Zheng, X.W., Schovsbo, N.H., Luo, Q.Y., Wu, J., Zhong, N.N., Goodarzi, F., Sanei, H., 2022. Graptolite reflectance anomaly. Int. J. Coal Geol. 261, 104072. https://doi.org/10.1016/j.coal.2022.104072.

Zhong, N.N., Qin, Y., 1995. Organic Petrology of Carbonate Rocks: Characteristics, Origin and Evolution of Macerals with Respects to Hydrocarbon Generation. Science Press, Beijing (in Chinese).

Zhou, Q., Xiao, X.M., Pan, L., Tian, H., 2014. The relationship between micro-raman spectral parameters and reflectance of solid bitumen. Int. J. Coal Geol. 121, 19–25. https://doi.org/10.1016/j.coal.2013.10.013.

Zhu, Y.H., Yang, X.Q., Yin, L., Qi, Y.P., 1998. Study of reflectance for the graptolites from lower Yangtze Region in Jiangsu, E China. Acta Palaeontol. Sin. 37 (3), 354–358. https://doi.org/10.19800/j.cnki.aps.1998.03.01.

Zou, C.N., Yang, Z., He, D.B., Wei, Y.S., Li, J., Jia, A.L., Chen, J.J., Zhao, Q., Li, Y.L., Li, J., Yang, S., 2018. Theory, technology and prospects of conventional and unconventional natural gas. Petrol. Explor. Dev. 45 (4), 604–618. https://doi.org/10.11698/PED.2018.04.04.

Zuo, Z.X., Cao, J., Hu, W.X., Shi, C.H., Wang, X.L., Yao, S.P., Luo, B., 2022a. Characterizing the maturity of highly evolved organic matter based on aromatic hydrocarbons and optimization with pyrobitumen reflectance and Raman spectral parameters. Sci. China Earth Sci. 65, 2335–2357. https://doi.org/10.1007/s11430-022-9955-7.

Zuo, Z.X., Cao, J., Wang, X.L., Luo, B., Zhong, Y., Li, K.Y., Hu, K., 2022b. Characterizing maturity of reservoir pyrobitumen with strong anisotropy: A calibration between reflectance and laser Raman spectral parameters. AAPG Bull. 106, 1373–1401. https://doi.org/10.1306/02032221049.